SPECIAL EDITION 2007 VOLUME 14 • NO. 2

NATIONAL HIGH MAGNETIC FIELD LABORATORY

MAG LAB REPORTS

FLORIDA STATE UNIVERSITY • UNIVERSITY OF FLORIDA • LOS ALAMOS LAB

Reviewing the 2006 NHMFL RESEARCH REPORTS

RESEARCH HIGHLIGHTS FROM:

Life Sciences
Chemistry
Magnet Science & Technology
Condensed Matter

Published by:
National High Magnetic Field Laboratory
1800 East Paul Dirac Drive
Tallahassee, Florida 32310-3706

Tel: 850 644-0311
Fax: 850 644-8350
www.magnet.fsu.edu

Director: GREG BOEBINGER
Director, Public Affairs: SUSAN RAY
Editing and Writing: AMY WINTERS, SUSAN RAY
Art Direction and Production: WALTER THORNER

This document is available in alternate formats upon request. Contact Amy Winters for assistance. If you would like to be added to our mailing list, please write us at the address shown at left, call 850 644-1933, or e-mail winters@magnet.fsu.edu.

2006 Year in Review

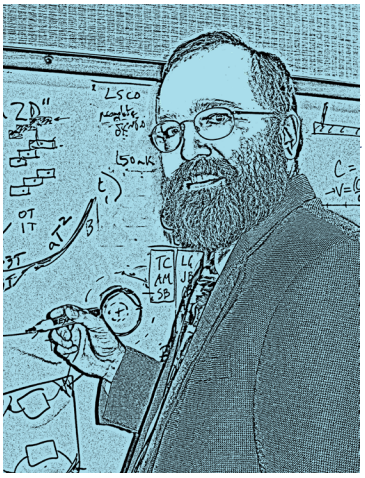

GREG BOEBINGER

Naturally, the most rewarding aspect of directing the National High Magnetic Field Laboratory is seeing the research productivity of our user programs. The annual research reports from our users have been rolling in these past few months, and the voluminous NHMFL Annual Report provides an accurate 'snapshot' of all user activities at the MagLab's world-leading high magnetic field research facilities during the past year.

This special edition of MagLab Reports is a little easier to digest than our exhaustive (and exhausting) Annual Report, as it provides to our general readership an overview of the highlights of the NHMFL Annual Report. This issue gets to the heart of why the MagLab exists: To serve as a resource for producing the best science in high magnetic fields. With seven user programs and three sites, I think you will agree that the MagLab enables an incredible and impressive array of scientific research.

In 2006, 398 research reports were received in 17 categories, representing the life sciences, chemistry, magnet science and technology, and condensed matter physics.

- ***In 2006, 398 research reports were received in 17 categories, representing the life sciences, chemistry, magnet science and technology, and condensed matter physics.***

Twenty percent of the research activities (78 reports) were already published in 2006, many in prominent journals such as the *Analytical Chemistry, Applied Physics Letters, Biochemistry, Energy & Fuels, IEEE Transactions on Applied Superconductivity, Journal of Magnetic Resonance, Journal of the American Chemical Society, Physical Review B, Physical Review Letters, Nature, Science and the Proceedings of the National Academy of Sciences.*

In addition to the 20% of the reports that have already resulted in publications, 6% of the reports cover results that have been accepted for publication; 11% are submitted for publication; and 37% have manuscripts in preparation. Together, these statistics account for roughly three-quarters of the total number of reports, with the rest representing on going research projects.

The majority of user research projects at the MagLab were funded by the National Science Foundation, the Department of Energy, and the National Institutes of Health. Other funding organizations include: The American Chemical Society, Children's Miracle Network, Christopher Reeve Paralysis Foundation, Engineering and Physical Sciences Research Council (UK), IBM, NASA, National Sciences and Engineering Research Council (Canada), Russian Foundation for Basic Research, U.S. Air Force Office of Scientific Research, U.S. Army, U.S. Navy, and the U.S. Geological Survey.

This MagLab's In-House Research Program (IHRP) - which encourages collaborations among internal and external investigators – supported 47 of the 398 research activities and was the primary support for 23 of the projects. The IHRP promotes bold but often risky efforts, many of which lead to enhancements in existing user facilities or to new technique development for the benefit of our user programs.

Winnowing down nearly 400 reports for a highlights issue is no simple task. Each report was reviewed by MagLab scientists. Of that number, 56 were recommended by the Magnet Lab Science Council, chaired by Dr. Lev P. Gor'kov, to be denoted as "2006 Research Highlights", and 30 reports were ultimately chosen for this special edition of MagLab Reports.

The selection criteria emphasized research that was published, featured new techniques for users and showcased outstanding research that together spans all three MagLab sites and seven user facilities. The reports that were recommended but not selected have been flagged as promising work to be followed closely in 2007.

Finally, each and every one of the user reports and resulting publications is available on our website, www.magnet.fsu.edu/usershub/publications. You can search by User Facility, Journal, First Author or Principal Investigator. In addition to the 2006 user reports and publications, you can pull up all MagLab user reports since 2004 and all publications dating back to 2000.

Without further *ado (or adieu)….voilà les* 2006 Research Highlights.

Rock 'n' Roll,

Greg Boebinger

Rapid and reliable recording of multidimensional NMR spectra is of great practical utility. An approach is presented that accomplishes this task by means of a covariance transform followed by a masking procedure that identifies and eliminates potential spectral artifacts. It is demonstrated for a two-dimensional total correlation spectroscopy (TOCSY) dataset of a decapeptide using only 48 increments along the indirect time domain.

This research was published in **Journal of the American Chemical Society**, **128**, 15564 (2006).

COVARIANCE NMR WITH MINIMAL DATASETS

Y. Chen (FSU, Physics & NHMFL), F. Zhang (NHMFL), W. Bermel (Bruker Biospin) and R. Brüschweiler (FSU, Chemistry & Biochemistry, and NHMFL)

INTRODUCTION

Covariance NMR spectroscopy [1] is an alternative method to 2D Fourier transform (2D FT) NMR to establish spin correlations in molecules. The covariance spectrum $\boldsymbol{C}$ is determined using the mixed time-frequency domain data $\boldsymbol{S}$, $\boldsymbol{C}=(\boldsymbol{S}^T\boldsymbol{S})^{1/2}$, where $\boldsymbol{S}$ is the N_1 x N_2 mixed time-frequency domain matrix after Fourier transform along the detection dimension t_2. The matrix square-root can be efficiently determined by singular value decomposition [2].

RESULTS AND DISCUSSION

An advantage of covariance spectroscopy over traditional 2D FT NMR is that the indirect dimension is not required to be sampled with a time increment that fulfills the Nyquist theorem, 1/(spectral width). Importantly, if N_1 is to be minimized to achieve maximal speed up, undersampling in t_1 can be advantageous by probing a wider range of t_1 evolution times. The conventional FT spectrum obtained from the time-domain of the same size (N_1=48) shows severe line broadening along the indirect dimension ω_1, and thus is unsuitable for simple analysis. The covariance spectrum has the same high resolution along both dimensions by definition. Comparison with the 2D FT spectrum with 2048 increments reveals, however, the presence of extra peaks reflecting the onset of poor sampling effects due to the small size of the dataset. These effects can be removed by a masking scheme that uses predicted spurious correlations caused by finite sampling. Application of the resulting mask to the covariance spectrum leads to the spectrum (upper left) that is essentially void of false peaks while most of the true peaks are present [3].

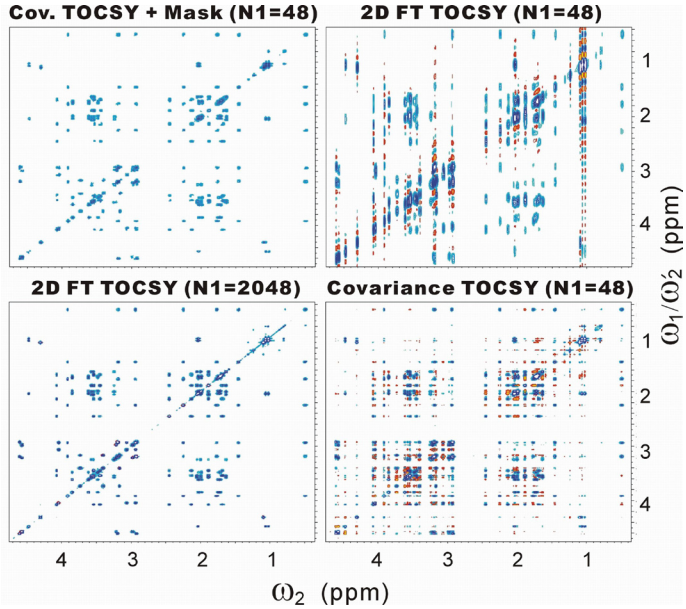

Figure 1.
Aliphatic proton region of TOCSY NMR spectra of 1 mM cyclic decapeptide antamanide in $CDCl_3$ collected at 800 data MHz proton frequency and 300 K.

CONCLUSIONS

The enhanced covariance method presented here provides high-resolution 2D spectra from minimal t_1 datasets. The undersampling and cross-validation schemes represent powerful means to suppress spurious correlations. The scheme, which offers substantial savings of measurement time for TOCSY- and COSY-type spectra, is readily applicable to high-throughput screening such as in metabolomics.

ACKNOWLEDGEMENTS

We thank Dr. David Synder for discussion. This work is supported by NIH (R01-GM066041).

REFERENCES

[1] Brüschweiler, R., *et al.*, J. Chem. Phys., **120** (2004) 5253-5260, Brüschweiler, R., J. Chem. Phys., **121** (2004) 409-414.

[2] Trbovic, N. *et al.*, J. Magn. Reson., **171** (2005) 277-283.

[3] Chen, Y. *et al.* J. Am. Chem. Soc., **128** (2006) 15564-11565.

LIFE SCIENCES

Sarcolipin (SLN) is a 31-residue alpha-helical protein that regulates Ca-ATPase, the enzyme that is responsible for calcium trafficking in heart muscle. In order to investigate the interaction between SLN and Ca-ATPase the topology of SLN in a native-like lipid environment was first deduced. From experiments conducted at the MagLab using low-E probe technology developed in-house, it was determined that SLN adopts a tilt of ~23 degrees, relative to the bilayer normal, and that the hydrophobic face of the protein is oriented facing the cytoplasmic surface of the lipid bilayer.

This research was published in **Biochemistry, 45** (36), 10939-46 (2006).

TWO-DIMENSIONAL NMR SPECTROSCOPY OF SARCOLIPIN IN ORIENTED LIPID BILAYERS

J.J Buffy (U. of Minnesota), N.J. Traaseth (U. of Minnesota), and G. Veglia (U. of Minnesota).

INTRODUCTION

Sarcolipin (SLN), a 31 amino acid integral membrane protein, regulates SERCA1a and SERCA2a, two isoforms of the sarco(endo)plasmic Ca-ATPase, by lowering their apparent Ca^{2+} affinity and thereby enabling muscle relaxation. Previous 1D solid-state NMR experiments on selectively ^{15}N-labeled sites showed that SLN crosses the lipid bilayer with an orientation nearly parallel to the bilayer normal. With a view toward the characterization of SLN structure and its interactions with both lipids and SERCA, we started the analysis of SLN in mechanically oriented DOPC/DOPE lipid bilayers as mapped by two-dimensional ^{15}N PISEMA experiments.

EXPERIMENTAL

NMR experiments were performed on a Bruker DMX-600 operating at a frequency of 600.14 MHz for ^{1}H and 60.82 MHz for ^{15}N. Prior to ^{15}N data acquisition, the integrity of the oriented lipid bilayer was verified using ^{31}P NMR. PISEMA experiments [1] were performed on a probe designed and constructed at the National High Magnetic Field Laboratory. In order to reduce sample heating, the probe utilizes a separate, low inductance ^{1}H resonator outside the ^{15}N detection coil. Typical NMR parameters used in the PISEMA experiments include a ^{1}H pulse length of 3.7 us, decoupling field of 50 kHz, rf field strengths of 48 kHz for ^{1}H and 67.6 kHz during the SEMA element, and a recycle delay of 3.5-5 s. PISEMA spectra on selectively ^{15}N-labeled SLN were acquired at 5°C with 9-12 t_1 increments and ~3k scans, while uniformly ^{15}N-labeled SLN samples required 32 t_1 increments and ~2k scans. .

RESULTS AND DISCUSSION

PISEMA spectra mapped the structure and topology of SLN in oriented DOPC/DOPE bilayers. Under our experimental conditions, this single-pass membrane protein adopts a helical conformation and crosses the membrane with a tilt angle of ~ 23°. PISEMA spectra obtained with both uniformly and selectively ^{15}N-labeled SLN clearly indicate a preferential orientation of the helix face containing Leu-21, Leu-25, and Ile-14 pointing towards the N-terminal side of the membrane, corresponding to the cytoplasm side in SR. Remarkably, PISEMA spectra suggest a topological interconversion on a slow time scale (i.e., slower that 10^{-4}s) with the presence of a second population of resonances. This additional population exhibits roughly the same tilt angle (θ) of the SLN helix with respect to the membrane bilayer, but a slightly different rotational angle (ρ). These two topologies may represent the two states whose

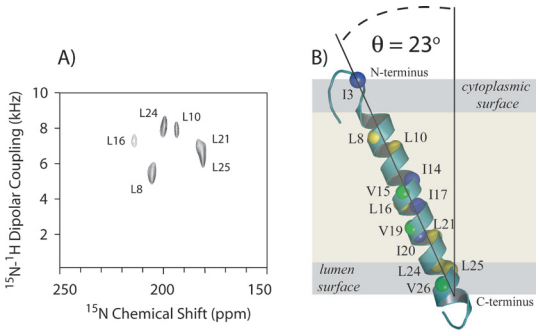

Figure 1.
A) PISEMA assignment for ^{15}N-Leu SLN in oriented lipid bilayers. The Leu spectral pattern follows the PISA wheel of the U-^{15}N SLN PISEMA. B) Proposed structural model of SLN in lipid membranes. The Leu, Ile and Val residues that were assigned in the PISEMA spectra are highlighted in yellow, blue and green spheres, respectively. SLN backbone is rotated around its helical axis so that the face containing Leu-21, Leu-25, and Ile-14 points toward the N-terminal side of the membrane.

information is totally lost in the isotropic micellar environments and may represent a pre-equilibrium state of SLN that constitutes a requirement for SERCA recognition.

CONCLUSIONS

SLN crosses the lipid bilayer with an angle of approximately 23°, echoing the conclusions of a similar investigation carried out with phospholamban (another Ca-ATPase inhibitor) under identical experimental conditions. This result demonstrates that high homologous primary sequences are likely to have the same interactions with lipid bilayers.

ACKNOWLEDGEMENTS

Many thanks to Dr. T. Cross for many helpful discussions. This work was supported by the National Institutes of Health Grant GM64742 and K02HL080081 to GV. J.J.B. is supported by the MinnCResT (NIDCR 5T32-DE007288-10); and N.J.T. pre-doctoral fellowship (AHA 0515491Z). The spectroscopy was performed at the NHMFL supported by NSF through cooperative agreement DMR-0084173 and by the State of Florida.

REFERENCES

[1] Buffy, J.J., *et al.*, Biochemistry **45** (36) (2006) 10939-46.

More than half of all human proteins are modified by the attachment of sugar chains that modify the biological function and enhance the blood stability compared to non-glycosylated proteins. Structural studies of these glycosylated proteins using high-field magnets such as are available at the National High Magnetic Field Laboratory require large amounts of pure samples that are enriched in stable ^{13}C and ^{15}N isotopes, but preparing these samples is very expensive. The high cost associated with these studies has discouraged researchers from studying these proteins. A broadly applicable strategy is developed for significantly reducing the cost of preparing these samples, which will facilitate structural and functional studies on this important class of proteins.

This research was published in **Journal of Biomolecular NMR, 36** (4) 225-233 (2006) and supported by the **In-House Research Program** (PI, Tim Logan).

ISOTOPE ENRICHMENT IN EUKARYOTIC CELLS AS A PRELUDE TO GLYCOPROTEIN STRUCTURAL BIOLOGY

W.J. Walton (FSU, Molecular Biophysics), D.Q. Ni (Molecular Biophysics) and T.M. Logan (Molecular Biophysics and Chemistry & Biochemistry, Florida State University)

INTRODUCTION

The genetic code in all organisms provides a template for producing proteins and RNA molecules that effectively "run" the cell and control nearly all aspects of the cell's fate. To expand the scope of the genetic code, many of the protein and RNA products are modified during or after biosynthesis. These post-translational modifications are particularly important in modifying or regulating protein and RNA activity. Covalent modification by attaching carbohydrates, either as single sugars or as complex chains, is the most prevalent of these post-translational modifications, being found on more than half of all proteins coded for in the human genome.

Despite the prevalence and importance of glycosylation in protein biochemistry, we know very little about how glycosylation affects protein structure because these proteins typically present more significant challenges to structural biology than even membrane proteins. One of the most daunting challenges is to produce large quantities of isotopically enriched, pure recombinant glycoproteins for NMR spectroscopy. As the foundation for a research program directed towards glycoprotein structural biology, we are focusing our initial studies on how to enhance isotope labeling in recombinant glycoproteins produced in insect cells or in mammalian cells.

EXPERIMENTAL

We use Thy-1 fused to green fluorescence protein (Thy-1-GFP) in these studies. The GFP "tag" provides very sensitive detection, which allows us to work with reasonable amounts of cells. Our approach is to obtain "partial" medium commercially and then supplement these media with isotopically enriched precursors.

RESULTS AND DISCUSSION

We demonstrated that isotopically enriched ammonium chloride can be metabolically incorporated into amino acids, which can then be used to synthesize recombinant glycoproteins produced in cultured insect Sf9 cells [1]. We also found that isotopically enriched glucose is readily incorporated into the sugar moieties of glycoproteins (which was not unexpected) and into several amino acids (which was unexpected).

Thy-1-GFP is produced at significantly higher levels in cultured mammalian cells and we are currently investigating similar approaches to isotope labeling in these cells. Our strategy is to identify growth media that can economically introduce labeled precursors, such as glucose and glutamate, that can be metabolized into amino acids and incorporated into recombinant proteins. Our preliminary experiments indicate that slowing metabolism results in significantly increased recombinant protein yields and are working towards repeating these experiments with isotopically enriched precursors.

CONCLUSIONS

In the past year we completed a study investigating the supplementation of insect cell growth medium with labeled glucose and ammonium chloride. The approach yielded fairly uniform labeling at a fraction of the cost of purchasing complete, isotopically enriched growth medium and should find utility in drug screening, structural studies, and biophysical studies. Labeling in mammalian cells will require additional supplementation of isotopically-enriched essential amino acids, but our preliminary studies are encouraging and should lead to significantly improved methods for producing isotopically enriched glycoproteins for structural biology.

REFERENCES

[1] Walton, W.J., *et al.,* Journal of Biomolecular NMR, **36** (2006) 225-233.

Membrane proteins are particularly difficult to structurally characterize and yet they represent the majority of all drug targets for today's pharmaceuticals. No matter what structural approach is used, sample preparation is the critical step. Using several examples of membrane proteins, we demonstrate that high quality samples can be prepared for solid-state NMR spectroscopy. This technology has the unique advantage of being able to characterize membrane protein structure in a membrane mimetic environment that is very similar to that of the native membranes.

This research has been accepted to publish in the **Journal of the American Chemical Society** .

UNIFORMLY ALIGNED FULL-LENGTH MEMBRANE PROTEINS IN LIQUID CRYSTALLING LIPID BILAYERS FOR STRUCTURAL CHARACTERIZATION

C. Li; P. Gao; H. Qin; R. Chase; T.A. Cross (FSU, Chemistry and Biochemistry, NHMFL); P. Gor'kov; W. Brey; (FSU, NHMFL)

INTRODUCTION

Progress has recently been made in membrane protein structure determination in lipid bilayer environments using solid state NMR spectroscopy of uniformly aligned samples. From the complete structure of gramicidin in 1993 to the structure of the M2 transmembrane domain with and without the antiviral drug amantadine, the structure of MerF, etc., there are ten membrane protein structures in

the Protein Data Bank characterized by aligned sample solid state NMR. Recent improvements in RF probe technology and in sample preparation have made it possible to obtain spectra of uniformly aligned full-length membrane protein samples. Here, we demonstrate the uniform alignment of three such proteins as well as the observation of characteristic resonance patterns for their transmembrane (TM) α-helices.

RESULTS AND DISCUSSION

Fig. 1 shows the PISEMA spectra of KdpF, Rv1861, and DAGK in liquid crystalline lipid bilayer environments. Here PISA wheels reflecting the helical topology are clearly observed for two (KdpF and Rv1861) of the three proteins. The third protein, DAGK has TM helices displaying small tilt angles such that the PISA wheel, which disappears at a 0° tilt angle, is unresolved in the uniformly ^{15}N labeled sample.

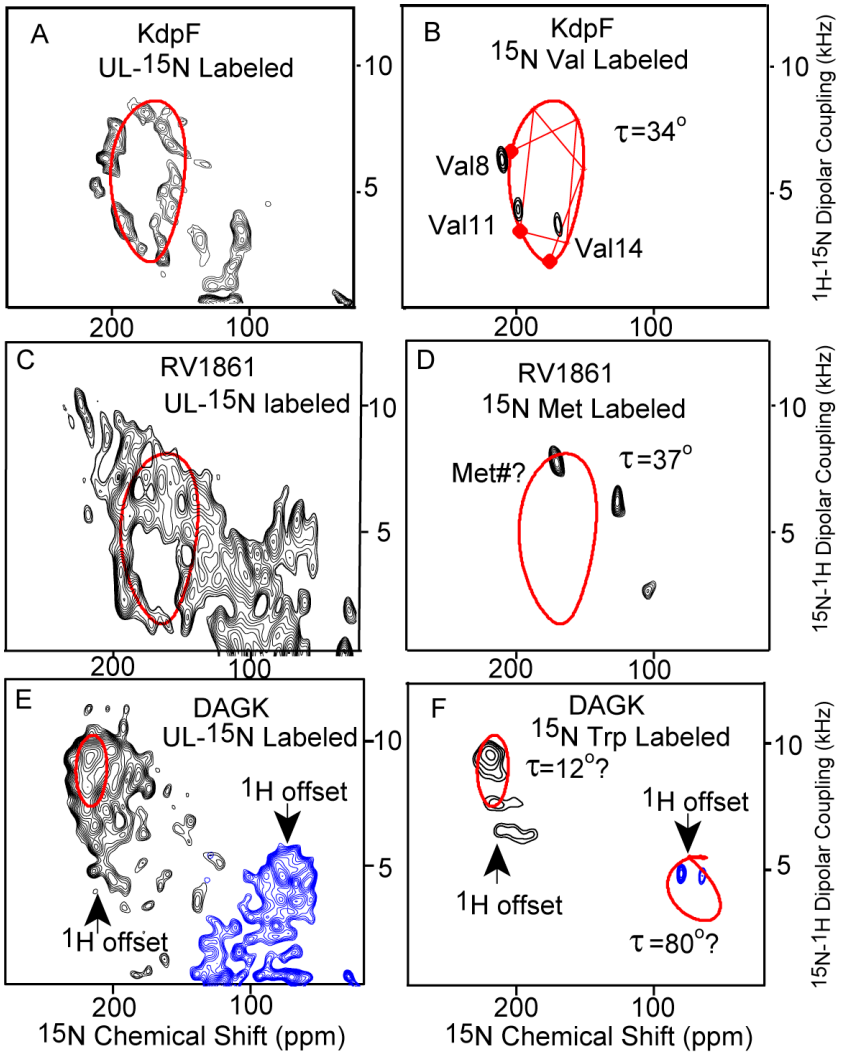

Figure 1.
PISEMA spectra of KdpF (A&B), Rv1861 (C&D) and DAGK (E & F) of uniformly ^{15}N-labeled (A,C&E) and amino acid specific labeled protein (B,D&F) expressed in *E. coli* and reconstituted into a mixture of lipids – dimyristoylphosphatidylcholine (DMPC) and phosphatidyl-glycerol (DMPG) in a 4:1 molar ratio. The samples were aligned between glass slides . Spectra were obtained at 600 MHz except for the ^{15}N UL KdpF spectrum which was obtained in the UWB 900 MHz magnet at the NHMFL using NHMFL Low-E probes. The low-electric field feature was essential for this spectroscopy. 0.8 ms cross polarization contact time, an acquisition time of 4 ms during with SPINAL decoupling was applied, and a recycle delay of 6 s were used. To avoid the limitations of the ^{1}H bandwidth the spectra of DAGK were obtained in two halves with different offset frequencies. The PISA wheels were calculated using motionally averaged dipolar ($\nu_{||}$ = 10.375 kHz) and chemical shift tensors (σ_{11} = 57; σ_{22} = 81; σ_{33} = 228 ppm).

CONCLUSION

Proteins ranging in molecular weight from a 3.5 kDa monomer to a 40 kDa trimer and an 82 kDa octamer have been uniformly aligned between glass slides demonstrating the feasibility of preparing full length membrane protein samples for solid state NMR structural characterization.

ACKNOWLEDGEMENT

This work was supported in part by NIH, GM 64676.

LIFE SCIENCES

The classical role of carbonic anhydrase (CA) is to maintain tissue pH homeostasis through acid-base reactions. Skeletal muscle contains at least four isozymes of CA (CA II, CA III, CA IV, and CA V). The roles of CA II, CA IV, and CA V are to accelerate the removal of acid as CO_2, transport lactate across the muscle membrane, and to fasten the metabolism of pyruvate, and are all well described. Surprisingly, the function of the most concentrated CA in muscle (CA III) has been a mystery until now. Using noninvasive ^{31}P magnetic resonance spectroscopy, MagLab scientists in collaboration with investigators from the University of Pennsylvania, have monitored muscle bioenergetics in real time from mice lacking muscle CAIII. These studies have uncovered that CA III plays an important role in mitochondrial ATP synthesis in muscle.

This research was published in **Proceedings of the National Academy of Sciences U.S.A, 104**, 371-376 (2007).

A QUANTITATIVE STUDY OF BIOENERGETICS IN SKELETAL MUSCLE LACKING CARBONIC ANHYDRASE III BY ^{31}P MAGNETIC RESONANCE SPECTROSCOPY

M. Liu (UF, Physical Therapy); G.A. Walter (UF, Physiology); N. Pathare (UF, Physical Therapy); U-J. Zimmerman (UPENN, Physiology); R. E. Forster (UPENN, Physiology); K. Vandenborne (UF, Physical Therapy)

INTRODUCTION

Oxidative slow skeletal muscle contains carbonic anhydrase III in a concentration as high as 2% of wet weight, but its primary function remains in question. In order to determine if the lack of this enzyme handicaps energy metabolism and/or acid elimination under stress, we measured the intracellular pHi and energy phosphates by ^{31}P magnetic resonance spectroscopy (MRS) in hind limb muscles of wild type and CAIII knockout mice during and after ischemia and intense exercise (electrical stimulation).

EXPERIMENTAL

The MR measurements were performed inside an 11T/470 MHz spectrometer. Spectra were acquired using a 6-mm x 12-mm oblong phosphorus (190.5 MHz) surface coil, placed over the belly of the gastrocnemius muscles. Spectra were acquired with a 50 µs square pulse, a pulse repetition time of 2 sec, and data were averaged into 30 second bins. Phosphorus spectra were obtained at rest (5 min), during ischemia (30 min) or electrical stimulation (2 min), and the following recovery (30 min). Intracellular pH was calculated based on the chemical shift of Pi. The Pi and PCr concentrations were determined using area integration.

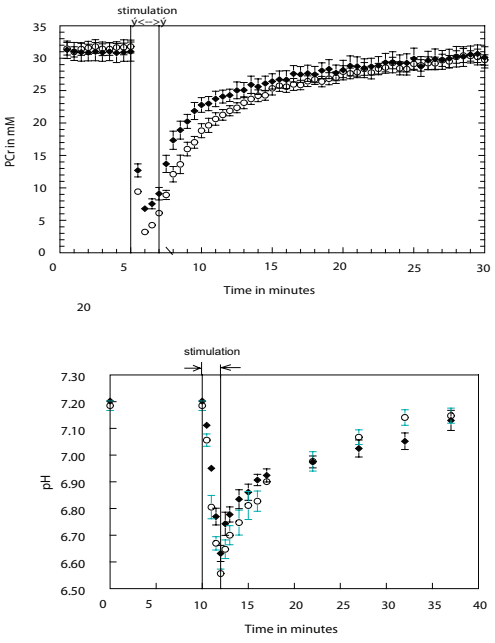

Figure 1.
PCr and pH kinetics in CA III knockout and wild type mice following electrical stimulation.

RESULTS AND DISCUSSION

Thirty minutes of ischemia caused phosphocreatine (PCr) to fall and inorganic phosphate (Pi) to rise, while pH and ATP remained constant in both strains of mice. PCr and Pi kinetics during ischemia and recovery were not significantly different between the two genotypes. From this we conclude that under neutral pH conditions resting muscle anaerobic metabolism, the rate of the creatine kinase reaction, intracellular buffering of protons, and phosphorylation of creatine by mitochondrial oxygen metabolism are not influenced by the lack of CA III. Two minutes of intense stimulation of the mouse gastrocnemius caused PCr, ATP and pH_i to fall and ADP and Pi to rise and these changes, with the exception of ATP, were all significantly larger in the animals lacking CA III. The rate of return of pH_i and ADP to control values was the same in wild type and mutant mice, but in the mutants PCr and Pi recovery were delayed in the first minute after stimulation (Figure 1).

CONCLUSIONS

Our quantitative study of muscle bioenergetics in CA III knockout mice showed a significant decrease in PCr recovery rate following electrical stimulation. We conclude that a lack of CA III impairs mitochondrial ATP *in vivo* synthesis.

ACKNOWLEDGEMENTS

This research was supported by NIH grant AR45394. The mutant mice were obtained from G. Kim and R. L. Levine at NIH. MR data were supported through the National High Magnetic Field Laboratory and obtained at the Advanced Magnetic Resonance Imaging and Spectroscopy (AMRIS) facility in the McKnight Brain institute of the University of Florida.

Plants, animals, and micro-organisms use chemicals for communication and defense. Learning these chemical languages provides new biological insights that improve our understanding of how biological species interact in their environment. In many cases, chemicals that are used for a specific biological function can be adapted for human medicinal or pesticide applications. About 25% of prescription drugs for humans are directly derived from these natural product chemicals and about another 25% of our drugs are modifications based originally on naturally occurring compounds. The major difficulty in discovering the identity of natural products is the large amount of material needed for NMR analysis. As demonstrated on the analysis of the venom from a single walkingstick insect, the 1-mm HTS NMR probe developed at the NHMFL has about 20x more sensitivity than conventional technology and can provide a significant new tool for natural product discovery.

This research was published in **ACS Chemical Biology, 1** (8), 511-514 (2006).

SINGLE INSECT NMR: TECHNOLOGY LEADING TO NEW SCIENCE

A. T. Dossey (UF, Biochemistry); S. S. Walse (USDA Laboratory); J. R. Rocca (UF, AMRIS); A. S. Edison (UF, Biochemistry)

INTRODUCTION

Due to analytical limitations, multiple animals or plants are typically required to identify natural products. Using a unique 1-mm high-temperature superconducting NMR probe developed at the NHMFL (1), we directly examined the chemical composition of defensive secretions from individual walkingstick insects. We found that the Florida walkingstick *Anisomorpha buprestoides* secretes similar quantities of glucose and mixtures of monoterpene dialdehydes that are stereoisomers of dolichodial. Different individual animals produce different stereoisomeric mixtures, the ratio of which varies between individual animals raised in the same container and fed the same food. Another walkingstick from Peru, *Peruphasma schultei*, also secretes glucose and a single, unique stereoisomer that we named "peruphasmal".

LIFE SCIENCES

EXPERIMENTAL

Adult A. *buprestoides* were collected at night in Gulf Hammock, Florida during the fall of 2005. Eggs produced by the insects were hatched in captivity. The young phasmids were fed a diet of only variegated *Ligustrum sinense* purchased from a local plant nursery. We were able to collect single milkings from half-grown males consisting of about 1 µL of a whitish fluid by gently touching the secretory duct with a glass pipette. To this we added 10 µL D_2O and without purification or additional preparation, we were able to collect the 1D ^1H NMR spectrum in Fig. 1 within about ten minutes following the milking. Complete assignments were done with standard 2D NMR experiments from the same sample.

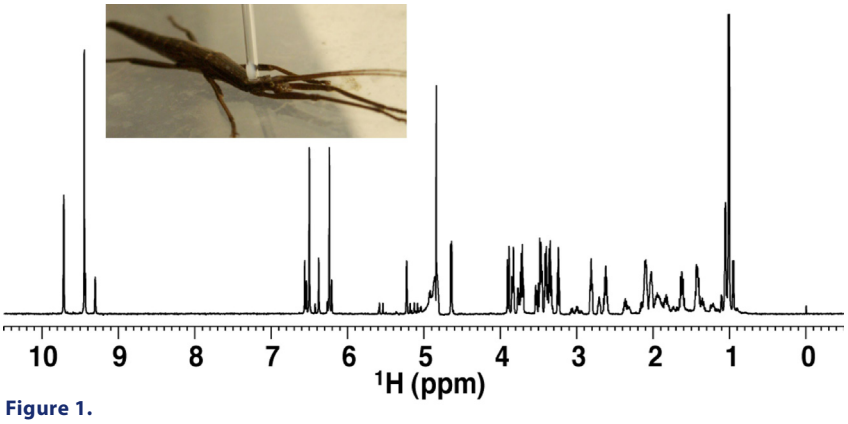

Figure 1.
1D 1H NMR spectrum from the 1-mm HTS probe of a single walkingstick milking as shown in Figure 3. The spectrum was collected in less than 1 minute with 8 scans and less than 10 minutes after the milking.

RESULTS AND DISCUSSION

1) We were able to obtain very high quality NMR data from the milking of a single insect (2). Previous studies on the same insect required over 1000 milkings (3).
2) We observed glucose in the defensive secretions (2). This was not previously observed, because samples were extracted into organic solvents.
3) The active component of the defensive spray is present as three different stereoisomers in the Florida insect but only a single isomer in the Peruvian species. Surprisingly, the composition of the stereoisomers changes between individual insects and as a function of time.

CONCLUSIONS

Traditionally, natural product studies consist of samples collected from hundreds or thousands of individuals. This was the first study to use NMR to analyze natural products from a single insect. The variability in isomers suggests new fertile ground in chemical biodiversity.

ACKNOWLEDGEMENTS

Bill Brey (NHMFL), Saikat Saha (NHMFL, now GE) Rich Withers (Bruker, now Varian), and Rob Nast (Bruker, now Varian) made the 1-mm HTS probe. Funding was from the HFSP, NIH, and NHMFL.

REFERENCES

[1] Brey, W. *et al.*, Journal of Magnetic Resonance **179** (2006) 290-3.
[2] Dossey, A. T. *et al.,* ACS Chemical Biology, **1** (8) (2006) 511–514.
[3] Meinwald, J. *et al.*, Tetrahedron Letters **1** (1962) 29-33.

MLR

To our knowledge, this is the first study that elucidates both the chemical and magnetic structure of a complex magnetic compound that would not have been possible without the utility of unique and powerful techniques developed at the NHMFL: high-field electron paramagnetic resonance (EPR) spectroscopy and Fourier transform ion cyclotron resonance (FT-ICR) spectrometry. EPR yielded the desired information on the orientation of the electron spins on the compound, a model five copper cluster, while FT-ICR showed how the various parts of the cluster are bonded together by looking at its fragmentation during infrared multiphoton irradiation. FT-ICR revealed also that the clusters are stable in solution, which is hard to accomplish by other techniques. The results obtained provide fundamentally new information on molecular magnetism, catalysis, and cluster stability, and demonstrate how seemingly diverse techniques provide synergies in solving a complex chemical problem. This work opens up a new window on the design of new molecular solids with desirable magnetic and catalytic properties.

This research was published in **Inorganic Chemistry, 44** (26), 9795-9806 (December 2005).

MAGNETIC AND VARIABLE FREQUENCY EPR STUDIES OF PENTA-NUCLEAR Cu^{2+} POLYOXOMETALATE

S. Nellutla (FSU, NHMFL), N.S. Dalal (FSU, NHMFL), J. van Tol (NHMFL), L.H. Bi (International University Bremen, Germany) and U. Kortz (International University Bremen, Germany)

INTRODUCTION

The class of Cu^{2+}-containing sandwich-type polyoxometalates is well-known and to date numerous complexes have been reported, but most of these polyanions are dimeric and contain three or four Cu^{2+}centers [1]. This report presents the magnetic properties and EPR spectroscopy [2] of a new penta-copper substituted polyoxoanion $[Cu_5(OH)_4(H_2O)_2(A\text{-}\alpha\text{-}SiW_9O_{33})_2]^{10-}$ (Cu_5). Cu_5 consists of two A-α-$[SiW_9O_{34}]^{10-}$ Keggin moieties which are linked via two adjacent W-O-W bonds and stabilized by a central $\{Cu_5(OH)_4(H_2O)_2\}^{6+}$ fragment leading to a structure with idealized C_{2v} symmetry (see Fig. 1). The Cu^{2+} ions in Cu_5 are at the corners of a rectangular pyramid.

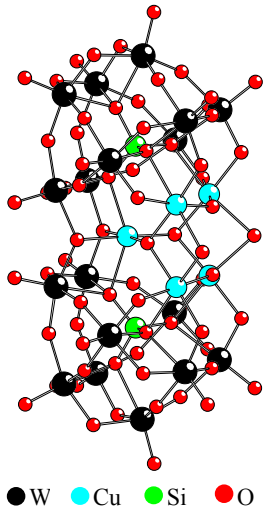

Figure 1.
Ball-and-stick representation of Cu_5.

EXPERIMENTAL

Magnetic susceptibility data were collected on Quantum Design MPMS XL SQUID Magnetometer and Q-band (~35 GHz) EPR data were collected on Bruker Elexsys 500 at the Department of Chemistry and Biochemistry, FSU. EPR measurements at high frequencies were done on a home-built homodyne instrument at the National High Magnetic Field Laboratory, Tallahassee, FL.

RESULTS AND DISCUSSION

Magnetic susceptibility data for Cu_5 is shown in Fig. 2. as a plot of χT vs T. Steady decrease of χT as temperature, T, decreases and suggests the presence of antiferromagnetic interactions between Cu^{2+} ions. Saturation below 50 K at ~0.39 emu-K/mol implies a spin $S_T = 1/2$ ground state, where S_T is the total spin value of the cluster. Analysis of the data according to the exchange spin Hamiltonian shown in Eq.1, provides the exchange constants as: $J_a = -51 \pm 6$ cm^{-1}, $J_b = -104 \pm 1$ cm^{-1}, $J_c = -55 \pm 3$ cm^{-1} and $g = 2.035 \pm 0.002$.

$$\hat{H}_{exch} = -2J_a [\hat{S}_1 \cdot \hat{S}_2 + \hat{S}_3 \cdot \hat{S}_4] - 2J_b [\hat{S}_1 \cdot \hat{S}_3 + \hat{S}_2 \cdot \hat{S}_4] - 2J_c [\hat{S}_1 \cdot \hat{S}_5 + \hat{S}_2 \cdot \hat{S}_5 + \hat{S}_4 \cdot \hat{S}_5 + \hat{S}_3 \cdot \hat{S}_5] \quad (1)$$

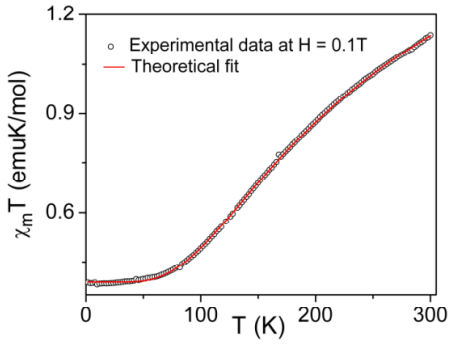

Figure 2. χT vs T for Cu_5.

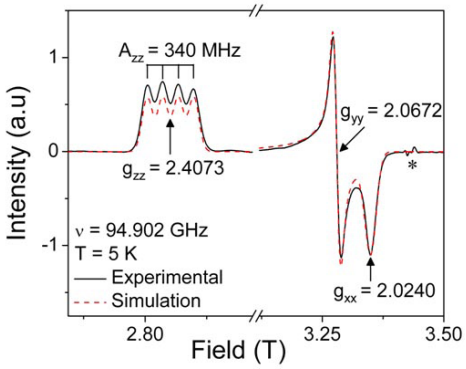

Figure 3. 95GHz EPR of Cu_5.

Figure 3 shows a 95 GHz powder spectrum of Cu_5 at 5 K and it is a typical Cu^{2+} spectrum, with a four line hyperfine structure (A_{zz}) on the low-field Zeeman peak (g_{zz}). The unpaired electron is assigned to the apical copper centre [2]. The spectra at all frequencies were reproduced satisfactorily with the Hamiltonian parameters: $g_{zz} = 2.4073 \pm 0.0005$, $g_{yy} = 2.0672 \pm 0.0005$, $g_{xx} = 2.0240 \pm 0.0005$, $|A_{zz}| = 340 \pm 20$ MHz (0.0113 cm^{-1}) implying that there is no net exchange field on the apical copper. The g-values are consistent with a $3d_{x^2-y^2}$ type molecular orbital ground state, as expected for a Cu^{2+} in an elongated rhombic-octahedral co-ordination with oxygen. A qualitative analysis of the g- and A_{zz} values, using the Crystal field – Molecular orbital theory [3], yields $\alpha^2 = 0.71$, where α is the molecular orbital coefficient of the ground state, indicating a moderate (~ 30%) contribution from the oxygen orbitals.

CONCLUSIONS

Magnetic and EPR measurements reveal that the pentameric copper core of Cu_5 exhibits strong antiferromagnetic interactions resulting in a spin $S_T = ½$ ground state, with a localized unpaired electron spin density. Cu_5 can therefore be considered as a model system for a 5-spin electronically coupled, spin-frustrated system.

ACKNOWLEDGEMENTS

NSF (NIRT), # DMR 0103290 and CHE-99-09502 for support.

REFERENCES

[1] see for e.g.: Kortz, U. *et. al.* Inorg. Chem.**40** (2001) 4742.
[2] Nellutla, S. *et. al.* Inorg. Chem.**44** (2005) 9795.
[3] Hathaway, B. J. *et. al.* Coord. Chem. Rev. **5** (1970) 143.

Membrane-associated proteins hold the secrets to many basic biological processes, as well as to the development of new drugs and vaccines. Because these proteins neither crystallize nor dissolve in water, however, very few of their structures are known. "Low-E" probes recently developed at the MagLab are being combined with new NMR techniques to map the structure of these proteins in their native environment. This study shows that Low-E probes are much less likely to damage the valuable protein sample than conventional probes.

This research was published in **Journal of Magnetic Resonance, 185**, 77-93 (2007) *and was supported by the* **In-House Research Program** (PI, William W. Brey).

COMPARISON OF SAMPLE HEATING IN SOLENOIDAL AND LOW-E NMR PROBES

P.L. Gor'kov, E.Y. Chekmenev, C. Li, W.W. Brey (NHMFL/FSU)

INTRODUCTION

Solid state NMR spectroscopy experiments expose the sample to high levels of high frequency electromagnetic field. Just as in a microwave oven, these fields will heat the sample. Excessive heating

may distort the NMR spectrum or even damage the sample. Recently introduced Low-E coil designs may reduce the level of heating [1]. A convenient way to quantify the improvement is to compare the values of RF input power required to produce identical 90° pulse lengths in a lossy biological sample (P_{bio}) and in a non-lossy reference (P_{nl}). The difference in input power $P_{heat} = P_{bio} - P_{nl}$ must then end up heating the biological sample. The same measurement can be done more precisely by comparing 90° pulse lengths (or RF fields $f_1 = \omega_1/2\pi$) measured with a lossy sample (τ_{90bio}) and with a non-lossy reference (τ_{90nl}) at the same power level P_{in}. Holding P_{in} constant eliminates the effect of errors that often accompany measurements of pulsed RF power. In the latter case, the fraction of RF input power diverted to sample heating can be expressed as:

$$\alpha_{heat} = \frac{P_e + P_m}{P_{bio}} = 1 - \frac{\tau_{90nl}^2}{\tau_{90bio}^2} = 1 - \frac{f_{1bio}^2}{f_{1nl}^2}$$

The loss factor α_{heat} alone should not be used to compare sample heating in different probes with different coils, or at different frequencies. A less efficient probe circuit with the same loss factor will deposit more power into the sample while achieving the same RF field f_1. For a heat sensitive sample, a spectroscopist should choose a probe with minimal heat deposition $q_{heat} = P_{heat}/f_{1bio}^2$, which is the cost of producing the required RF field f_1 in terms of power P_{heat} deposited in the sample. The heat deposition coefficient q_{heat} combines sample loss factor α_{heat} with probe circuit power efficiency η in the absence of sample loss:

$$\eta = \frac{f_{1nl}^2}{P_{in}} \qquad q_{heat} = \frac{\alpha_{heat} P_{in}}{f_{1bio}^2} = \frac{\alpha_{heat}}{1-\alpha_{heat}} \frac{P_{in}}{f_{1nl}^2} = \frac{\alpha_{heat}}{(1-\alpha_{heat})\eta}$$

Table 1.
Sample heating comparison between ^1H–^{15}N probes with low-E resonator and double-tuned 4-turn solenoid.

Field (MHz)	Probe	τ_{90nl} (µs)	τ_{90bio} (µs)	α_{heat}	η (kHz²/W)	q_{heat} (mW/kHz²)
400	4't solenoid	4.75	7.10	55 %	42.6	28.7
600	4't solenoid	5.05	9.55	72 %	37.7	68.2
600	low-E coil I	5.10	5.48	13 %	37.0	4.0
600	low-E coil II	5.75	6.23	15 %	29.1	6.1
900	low-E coil II	6.88	8.45	34 %	20.3	25.4

EXPERIMENTAL

Tests of sample heating by the ^1H field were conducted in five different probes designed for the same sample size but operating in magnets at three different fields. The results are summarized in Table 1. An applied ^1H power of 65 W was used in all cases. The 90° pulse length was measured for a non-lossy sample of pump oil and a typical biological sample described in [2]. Low-E resonators [1] using gaps of 6.4 (coil I) and 9.9 mm (coil II) were both tested, because the larger gap can produce a somewhat larger f_1 without arcing.

DISCUSSION AND CONCLUSIONS

The reduction in sample heating is illustrated by comparing the low-E probe to a conventional 4-turn solenoid at 600 MHz. RF power deposition in the biological sample has been reduced by 17 times in low-E coil I and by 11 times in low-E coil II. Coil I, with its smaller gap, is more efficient and produces the least sample heating. One might expect the ^1H power efficiency η of the low-E probe to be much worse than that of the solenoid due to the 3.3 times larger volume of the low-E resonator. However, the superior efficiency of the single resonance ^1H circuit in the low-E probe makes up for the difference in filling factor. As shown in Table 1, the low-E probe with coil I has the same ^1H efficiency as the double-tuned solenoid. The low-E probe with coil II is somewhat less efficient, which can be attributed to using more chip capacitors in the gap of the resonator. The amount of ^1H power dissipated in the bilayer sample in a 900 MHz low-E probe is 4 times larger than in its 600 MHz counterpart, yet it is still just 37% of that dissipated in the 4-turn solenoid at 600 MHz. To date, the aligned samples studied in the 900 MHz low-E probe have exhibited no signs of damage after demanding experiments. Yet because of the large rise of RF absorption at 900 MHz, it is important to

CHEMISTRY

invest in further refinements to the low-E coil for use at ultra-high NMR fields.

REFERENCES

[1] Gor'kov, P.L. *et al.*, J. Magn. Reson. **185** (2007) 77-93.
[2] Gor'kov, P.L. *et al.*, J. Magn. Reson. **181** (2006) 9-20.

Asphaltenes are a primary constituent of the residue remaining after the lower-boiling components of petroleum crude oil have been collected by distillation (gasoline, kerosene, lube oil, jet fuel, etc.). In a paper published in 2006 in *Energy & Fuels*, NHMFL's Geoff Klein, Ryan Rodgers, and Alan Marshall used ultrahigh-resolution mass spectrometry to define for the first time the detailed chemical composition (identification of thousands of chemically distinct components) of asphaltenes. They also showed that asphaltenes extracted physically (by temperature and pressure drop as crude oil is pumped out of a reservoir) differ qualitatively from those extracted chemically (by precipitation with heptane, an organic solvent). This paper thus provides the first rational basis for characterizing one of nature's most chemically complex mixtures.

This research was published in **Energy & Fuels, 20**, 1965-1972 (2006).

COMPOSITIONAL DIFFERENCES BETWEEN PRESSURE-DROP AND SOLVENT-DROP ASPHALTENES DETERMINED BY ELECTROSPRAY IONIZATION FT-ICR MASS SPECTROMETRY

G. C. Klein (FSU Chemistry & Biochemistry), S. Kim (NHMFL Tallahassee), R.P. Rodgers (NHMFL Tallahassee; FSU Chemistry & Biochemistry), and A. G. Marshall (NHMFL Tallahassee; FSU Chemistry & Biochemistry)

RESULTS AND DISCUSSION

Asphaltenes are typically defined by their solubility in benzene and insolubility in pentane or heptane. They are believed to exist in petroleum crude oil as colloidal suspension, stabilized by surface-adsorbed resins. Their normal equilibrium under reservoir conditions may be disrupted during production by pressure reduction, crude oil chemical composition changes, introduction of miscible gases and liquids, mixing with diluents and other oils, and acid stimulation, hot oiling, and other oilfield operations. In this work, we compare the compositional differences between heptane-precipitated asphaltenes and asphaltenes collected by live oil depressurization. Negative and positive ion electrospray yield the acidic and basic species, respectively. We find that the heptane-precipitated asphaltenes contain higher double bond equivalents (number of rings and double bonds) compared to the asphaltenes induced by pressure drop. On the other hand, the pressure drop product exhibits a higher abundance of species containing sulfur. Thus, the solubility criterion for asphaltenes defines a significantly different chemical composition (see Figure) than the (more field-relevant) pressure-drop criterion.

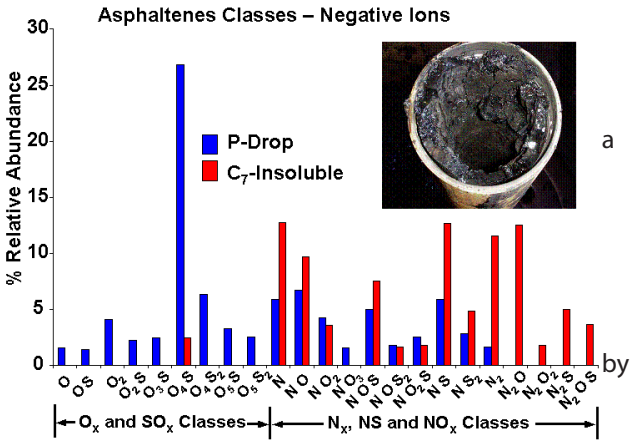

a

by

ACKNOWLEDGEMENTS

We thank Christopher L. Hendrickson and John P. Quinn for helpful discussions, and Daniel McIntosh for machining the custom parts required for the 9.4 T instrument construction. This work was supported by the NSF National High-Field FT-ICR Mass Spectrometry Facility (DMR 00-84173), Florida State University, and NHMFL.

REFERENCES

[1] Klein, G. C. *et al.*, Energy & Fuels **20**, (2006) 1965-1972.

Extinct radionuclides in the early solar system left behind isotope footprints from which a precise chronology of events can be constructed about how our solar system developed. In the report by Humayun et al., the new Plasma Analytical Facility of the Geochemistry group was utilized to study the distribution of the elements hafnium (Hf) and tungsten (W) in selected components of meteorites. A clear post-formation disturbance of the extinct chronometer, Hf-182, was found in the samples on which previous age determinations were based. New samples were identified for subsequent measurements to provide an improved chronology of the formation of the early Solar System by Hf-W dating techniques.

This research has been submitted to **Geochim Cosmochim Acta** *and is under revision.*

THE DISTRIBUTION OF Hf AND W IN INCLUSIONS FROM METEORITES AND CHRONOLOGY OF THE EARLY SOLAR SYSTEM

M. Humayun (FSU, Geological Sciences & NHMFL/Geochemistry); S. B. Simon, L. Grossman (U. Chicago, Geophysical Sciences)

INTRODUCTION

The birth of the solar system is marked by a rapid series of events that occurred within the first100 million years (m.y.) from the collapse of a molecular cloud core. Precise dating of events that occurred 4.56 billion years ago is challenging, and is best accomplished by radiometric clocks based on extinct chronometers, i.e. radionuclides that entirely decayed during the first 100 million years of solar system history. One of these chronometers is based on the beta decay of ^{182}Hf (produced in supernovae) to ^{182}W (stable), one of the five isotopes of tungsten, with a half-life of 9 m.y. (Kleine *et al.*, 2005). Application of the ^{182}Hf-^{182}W chronometer requires experimental determination of the initial ratio of ^{182}W/^{184}W in the solar system. The first objects to form as solids in the solar system are the calcium-aluminum-rich inclusions (CAIs) found in the carbonaceous chondrite meteorites. Kleine et al. (2005) reported the first ^{182}Hf-^{182}W ages on the CAIs and obtained an initial ^{182}W/^{184}W identical to that obtained from iron meteorites, implying the formation of the iron meteorites contemporaneously with the condensation of the first solids. This result is difficult to understand since individual chondrites accumulated over periods of several m.y., requiring that bodies large enough to form iron cores must have accumulated over longer periods of time. The meteorite from which the CAIs were obtained (Allende) had experienced a protracted history of post-accumulation disturbances which may have affected the ^{182}Hf-^{182}W ages in these CAIs. We explored this by analyzing the distribution of Hf, W and other elements in the individual minerals constituting CAIs using laser ablation ICP-MS at the NHMFL.

EXPERIMENTAL

Analyses of the distribution of Hf, W, and other elements were performed at the Plasma Analytical Facility at the NHMFL, using a New Wave UP213 UV laser ablation system coupled to a

CHEMISTRY

magnetic-sector ICP-MS (Thermo Finnigan Element1). Measurements were performed in line scan mode with 12 or 25 μm beam diameters, with the stage moved at 4-5 μm/s, 10 Hz laser repetition rate and 50% power output. The peaks ^{7}Li, ^{25}Mg, ^{27}Al, ^{29}Si, ^{34}S,^{43}Ca, ^{49}Ti, ^{53}Cr, ^{57}Fe, ^{60}Ni, ^{180}Hf, ^{181}Ta, ^{182}W, ^{183}W, ^{193}Ir, ^{195}Pt and ^{197}Au were acquired in low resolution (R=300) at 50 ms/peak (Humayun *et al*., 2006).

RESULTS, DISCUSSION & CONCLUSIONS

CAIs are composed of the minerals melilite (Ca-Al silicate), fassaite (Ca-Mg-Al-Ti silicate), spinel ($MgAl_2O_4$) and Fe-Ni metal. The distribution of the elements in CAIs was studied in two chondrites, Allende which had experienced post-accumulational heating, and Efremovka where these effects are relatively minor. The Efremovka CAIs had fairly simple elemental distribution patterns. All the W occurs in Fe-Ni metal grains (up to 1000 ppm), all the Hf occurs in fassaite (12-15 ppm), while melilite and spinel were found to contain negligible quantities (<0.010 ppm). In Allende, the Hf is hosted exclusively in fassaite, as well, but the W-host metal is absent. All Allende Fe-Ni metal has been altered into secondary oxides, sulfides, etc. W-rich veins were found in fassaite in Allende (Humayun *et al*., 2006). Such mobility is clear evidence for the post-formational disturbance of the ^{182}Hf-^{182}W chronometer in Allende. We find that the ambiguity in the results of Kleine *et al.* (2005) on the ^{182}Hf-^{182}W chronometry of the early history of the solar system could be resolved by new measurements on CAIs from the Efremovka meteorite.

ACKNOWLEDGEMENTS

This research was funded by NASA Cosmochemistry program.

REFERENCES

[1] Kleine, T., *et al.*, Geochimica et Cosmochimica Acta, **69** (2005) 5805-5819.
[2] Humayun, M., *et al.*, 38th Lunar Planet. Sci. Conf., Houston, Texas, abstract#2338 (2006).

Diffusion weighted magnetic resonance imaging (MRI) has become a sensitive clinical tool to detect tissue injury. Typically diffusion-weighted MRI is acquired by varying the magnitude and the direction of diffusion sensitizing gradients. However, additional information about tissue microstructure may also be obtained if the diffusion time is varied. In this report, MagLab scientists demonstrate that previously unrecognized structural information is obtainable from time dependent, *q*-space diffusion MR studies of biological tissues.

This research was published in **Journal of Magnetic Resonance, 183** (2), 315-23 (December 2006).

ANOMOLOUS DIFFUSION IN NERVOUS TISSUE AS A NOVEL MRI CONTRAST

E. Ozarslan, P.J. Basser (NIH); T.M. Shepherd (UF, Neuroscience); P.E. Thelwall (Newcastle U, England); B. Vemuri (UF, Computer Science); S.J. Blackband (UF, Neuroscience)

INTRODUCTION

Many biological tissues including the neural tissue have a hierarchical structure that exhibits significant self-similarity. Sensitizing the MR signal to random movements of the molecules makes it possible to probe length scales that can not be resolved by conventional MR imaging methods. Varying the diffusion time provides a means to observe water diffusion at different temporal or spatial scales. A nonlinear dependence of the mean-square-displacements (MSDs) on the diffusion time gives rise to anomalous diffusion, which occurs in systems exhibiting fractal behavior. In fractal environments [2], Brownian motion of particles are restricted in all length scales giving rise to the scaling relations $\langle r2 \rangle$

$dw\ t \propto 2\ /$, and $P(r = 0) \propto t{-}ds\ /\ 2$ where $<r^2>$ is the mean square displacement and $P(r=0)$ is the return to origin probabilities for the water molecules undergoing diffusion during time t. The scaling exponents dw and ds are called the fractal dimension of the random walk and the spectral (fraction) dimension respectively. The diffusion process is called "normal" if $dw=2$, where the cases $dw>2$ and $dw<2$ correspond to sub- and super-diffusion regimes (anomalous diffusion) respectively. These two scaling exponents are related to the fractal dimension, df, through the relationship $df=dw\ ds/2$. In one-dimensional q-space measurements, the projection of the propagator onto the axis is measured. Thus we have a one-dimensional space which can be quantified by the indices ds' and df'. We have performed experiments on excised rat hippocampi to examine this contrast.

EXPERIMENTAL

A series of diffusion-weighted MR images were acquired from three excised rat hippocampi with varying diffusion gradient strengths and diffusion times. The imaging parameters were: B0=14.1T, TR=1000ms, TE=12.6ms, resolution = (78x78x500)μm_3, matrix size=(64x64x3), δ=2ms. The diffusion gradient strength varied between 0 to 2935mT/m while the q-space acquisition was repeated 10 times with Δ values ranging from 12 to 300ms on a logarithmic scale.

RESULTS AND DISCUSSION

Figure 1 shows images generated of the scaling exponents. Different scaling behavior is observed in regions of the hippocampus. Contrast appears to be influenced by unique cytoarchitectural features of different hippocampal regions. For instance, the densely packed myelinated regions like the fimbria and the dorsal hippocampal commissure appear to be in the subdiffusive regime where the characteristic lengths associated with the diffusion process scales slowly in time.

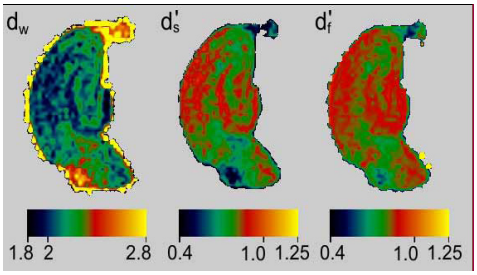

Figure 1.
Scaling exponent maps of isolated hippocampi.

CONCLUSIONS

The formalism developed to characterize diffusional processes in fractal environments was applied to q-space MRI data collected from excised neural tissue. The functional fits were very satisfactory indicating the appropriateness of the approach. This method can be used to understand the variability of data acquired with different values for diffusion time. The method also provides a novel contrast mechanism that may enhance the utility and specificity of diffusion weighted MRI/S to better assess the structural changes that occur during development and various neuropathologies and has been published (1).

ACKNOWLEDGEMENTS

Support was provided by NIH grant P41 RR 16105 and the National High Magnetic Field Laboratory.

REFERENCES.

[1] Ozarslan E *et al.*, J Magn Reson. **183**, 2, (2006) 315-23.

CHEMISTRY

Diffusion tensor imaging with magnetic resonance [1,2] has proven to be a very valuable tool for the study of structured material. This method allows tracking the fiber structure of complex material, like the human central nervous system. However diffusion tensor imaging only allows the resolution of simple structures and fails to accurately map crossing fiber structures in the central nervous system. To overcome this limitation, we have developed an accurate and fast method for fiber orientation mapping using multidirectional diffusion-weighted magnetic resonance data [3]. This new method, called the diffusion orientation transform (DOT), transforms measured diffusivity profiles into displacement probability profiles. Our method is based on the high-angular-resolution diffusion-weighted image (HARDI) acquisition scheme and can be extended to more general acquisition strategies. Our technique can be regarded as a transformation of diffusivity to probability profiles whose peaks correspond to distinct fiber orientations.

This research was published in **Neuroimage, 31** (3), 1086-1103 (2006).

RESOLUTION OF COMPLEX TISSUE MICROARCHITECTURE USING DIFFUSION ORIENTATION TRANSFORM

E. Ozarslan (UF Physics and National Institutes of Health), T. M. Shephard (UF, Neuroscience), B. C. Vemuri (UF Computer Information Science and Engineering), S. J. Blackband (UF, Neuroscience), and T. H. Mareci (UF, Biochemistry and Molecular Biology)

INTRODUCTION

We have developed an accurate and fast method for fiber orientation mapping using multidirectional diffusion-weighted magnetic resonance (MR) data [3]. This new method, called the diffusion orientation transform (DOT), transforms measured diffusivity profiles into displacement probability profiles. Our method is based on the high-angular-resolution diffusion-weighted image (HARDI) acquisition scheme and can be extended to more general acquisition strategies. Our technique can be regarded as a transformation of diffusivity to probability profiles whose peaks correspond to distinct fiber orientations.

EXPERIMENTAL

To test the performance of the DOT, we calculated the orientation probabilities with HARDI data from three anatomical regions of excised, perfusion-fixed rat nervous tissue (optic chiasm, brain and spinal cord). These experiments were performed with the approval of the University of Florida Institutional Animal Care and Use Committee. The images were acquired with either a 17.6 T (brain) or 14.1 T (spinal cord and optic chiasm) magnet

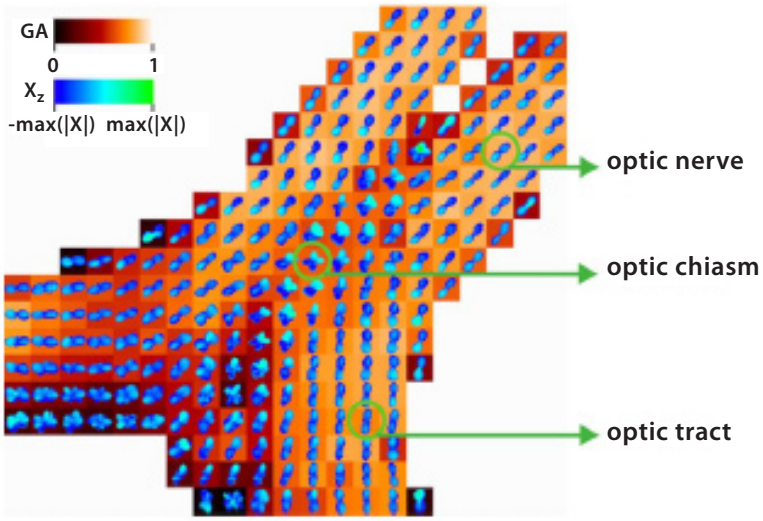

system. A diffusion-weighted spin echo pulse sequence was used. Diffusion-weighted images were acquired along 81 (brain) or 46 (spinal cord and optic chiasm) directions with a b-value of 1500 s/mm^2 (brain and spinal cord) or 1250 s/mm^2 (optic chiasm) along with a single image acquired at b –value of 0 s/mm^2.

RESULTS AND DISCUSSION

Our approach utilizes the Fourier transform relationship between the water displacement probabilities and diffusion-attenuated MR signal expressed in spherical coordinates. The radial part of the Fourier integral is evaluated analytically under the assumption that the MR signal attenuates exponentially. Orientation maps calculated from excised rat nervous tissue data demonstrate this technique's ability to accurately resolve crossing fibers in anatomical regions such as the optic chiasm (see figure). This methodology has a trivial extension to multi-exponential diffusion-weighted signal decay. The developed methods will improve the reliability of tractography schemes and may make it possible to correctly identify the neural connections between functionally connected regions of the nervous system.

CONCLUSIONS

The DOT technique provides a direct estimation of displacement probability surfaces within each voxel from multi-orientational diffusion-weighted MRI data. The method is robust, fast and can be implemented nonparametrically for direct estimation of probability values along desired directions or by using a spherical harmonic transformation that gives the Laplace series coefficients of the probability profile. In either case, high resolution probability surfaces can be reconstructed easily from the signal values. As demonstrated in excised rat nervous tissue, the potential applications of our approach include more accurate estimates of fiber orientations that will improve the existing fiber tractography schemes. This then could enable the reliable mapping of more connections between different parts of fibrous tissues.

ACKNOWLEDGEMENTS

Support provided by the NIH grants R01-NS42075, R01-NS36992 and P41-RR16105, UF Alumni Foundation, and the National High Magnetic Field Laboratory. MRI data were obtained at the AMRIS facility of the UF McKnight Brain Institute.

REFERENCES

[1] Basser, P. J., J. Mattiello, *et al.* (1994). "Estimation of the Effective Self-Diffusion Tensor from the NMR Spin Echo." Journal of Magnetic Resonance B **103**: 247-254.

[2] Basser, P. J., J. Mattiello, *et al.* (1994). "MR diffusion tensor spectroscopy and imaging." Biophys.J. **66**(1): 259-267.

[3] Ozarslan E, *et al.*, NeuroImage **31** (2006) 1086-1103

The choice of cable-in-conduit (CIC) conductor for the just approved Fusion Reactor, ITER, points to the need to properly understand one of the consequences of the excellent cooling that CIC conductors (also chosen for the NHMFL Series-Connected Hybrid designs too) possess - namely significant bending strains that can be developed by the Lorentz force in unsupported strand to strand crossovers in the cable. This issue has come to the fore as analysis of the very large ITER test coils has progressed. New designs of Nb_3Sn conductor with higher current density tend to have larger filaments too - the possibility of filament degradation, both reversible and irreversible under cyclic energization of the magnets is an important issue. The experiments of Takayasu enable study of these effects in sub-size cables and in strands under pure bending conditions. The first results already point to big differences in the mechanical behavior of otherwise rather similar conductors.

This research has been accepted for publication by **IEEE Transactions on Applied Superconductivity.**

CHARACTERIZATION OF NB_3SN SUPERCONDUCTING WIRES UNDER STRAIN: TRANSVERSE STRESS AND BENDING EFFECTS

M. Takayasu, L. Chiesa, A. Allegritti, and J.V. Minervini (Massachusetts Institute of Technology, Plasma Science and Fusion Center)

INTRODUCTION

In order to study degradations due to transverse strain and bending effects on Nb_3Sn superconducting conductors, we continued transverse stress tests on 36-strand cables, and single-strand pure bending tests using the 20 T, 195 mm bore high-field large-bore DC magnet.

TRANSVERSE STRESS EFFECT ON THE CRITICAL CURRENT OF 36-STRAND NB_3SN CABLES

We have developed a device to study the effect of transverse stress on a sub-sized Nb_3Sn cable using a mechanical load that simulates the Lorentz loads in ITER conductors. The test sample is a single turn (about 110 mm diameter) circular coil composed of 36 superconducting strands (cabling pattern of 3x3x4). The transverse stress is applied to the cable using a conical wedge that converts a vertical force into a radial (transverse) force. Two samples of IGC wire used for ITER CS model coil and newly developed high-performance wire (Outokumpu) were investigated [1]. The two samples showed quite different behaviors to the applied transverse loads. The high-performance strand cable showed a stronger sensitivity to the applied load than the old CS model coil wire. The transverse load effects of the new high performance wire have been intensively studied taking a sequence of loading and unloading operations at 15 T. The cable is sensitive to the mechanical applied load, showing 5-10% degradation for loads lower than 20 MPa. By 100 MPa stress, the cable critical current was degraded to ~30% of its initial, unloaded value. We will continue the transverse load tests for various Nb_3Sn strand cables to understand operation degradations of Nb_3Sn conductors.

SINGLE-STRAND VARIABLE PURE-BENDING

A variable bending test probe for a single strand was developed last year [2]. This year we modified the bending device to apply pure-bending only without axial strain to a strand sample [3]. This device allows applying pure bending up to 0.9% over the sample of about 100 mm length in liquid helium. Bending properties of new ITER high performance Oxford and Outokumpu wires were tested. The bending was applied first up to 0.2% (-0.2%) and then to the other direction up to 0.8%. The critical currents at 15 T of the Oxford and Outokumpu wires degrade from 175 A to 63 A and from 133 A to 67 A, respectively, by the bending of 0.8%. After the 0.8% bending the critical currents of the Oxford and Outokumpu wires were irreversibly reduced to 114 A and 105 A, respectively. These values were 65% of the initial value for the Oxford wire and 79% of the initial value for the Outokumpu wire. Note that the oxford wire was much more sensitive to the bending than the Outokumpu wire. The initial

critical currents of Oxford wire were much higher than that of the Outokumpu wire. However the critical currents at the 0.8% bending and also the reversible values resulted after 0.8% bending of these tested wires were very similar between the Oxford and Outokumpu wires. It is very important to figure out the high sensitivities against bendings and strains which are observed unexpectedly for the newly developed advanced Nb_3Sn wires.

ACKNOWLEDGEMENTS

This work was supported by the U.S. Department of Energy, Office of Fusion Energy Science under Grant Number: DE-FC02-93ER54186.

REFERENCES

[1] L. Chiesa, *et al.*, "Experimental studies of transverse stress effects on the critical current of a sub-sized Nb3Sn superconducting cable,' ASC 2006, 4LG03, Seattle, Washington, September 2006.

[2] D.L. Harris, "Characterization of Nb_3Sn superconducting strand under pure bending," MIT Mechanical Engineering master thesis, 2005.

[3] A. Allegritti, "Development and experimental test of a device for the measurements of the critical current of superconducting strands under pure bending conditions," University of Bologna, Department of Mechanical Engineering, Italy, 2006.

Solidification is well known to be a process in which many bad things can happen - segregation of alloying elements and impurities, development of porosity and the inhomogeneous distribution of defects. This makes it interesting to develop strategies that minimize such effects by coupling other sources of energy than just withdrawal of thermal energy that can positively homogenize the solidifying material. Evidently very high magnetic fields can be beneficial. In the electromagnetic acoustical treatment described here, a small amount of RF power applied in a 20 Tesla field greatly reduces segregation and avoids top to bottom microstructure differences.

This research has been accepted for publication in the **TMS 2007 Annual Meeting Symposium Proceedings**.

NON-CONTACT ULTRASONIC TREATMENT OF CONDUCTIVE MATERIALS IN A HIGH MAGNETIC FIELD ENVIRONMENT

J. B. Wilgen, R. A. Kisner, R. A. Jaramillo, G. Mackiewicz-Ludtka, and G. M. Ludtka (Oak Ridge National Laboratories)

INTRODUCTION

When induction heating is applied in a high magnetic field environment, the induction heating coil is typically configured in such a way that high intensity ultrasonic treatment occurs naturally. The resulting configuration is that of a highly effective electromagnetic acoustical transducer (EMAT). The synergistic interaction of a high surface current density (induced via induction heating) with the steady-state high magnet field results in an especially effective method for creating a high energy density acoustic environment. The exceptionally high energy efficiency of the resulting electromagnetic transducer is due to the use of a high magnetic field, which greatly reduces the current needed to achieve the same acoustic pressure. This provides an efficient non-contact method for applying high-intensity ultrasonic energy to the processing of conductive materials. Furthermore, the applied ultrasonic excitation can be uniformly distributed over most of the surface of the sample.

EXPERIMENTAL

A high-field EMAT has been used for non-contact ultrasonic processing of aluminum samples (35 mm diameter x 52 mm long) during solidification. The magnetic field for the EMAT was supplied by a 20 Tesla resistive magnet located at the National High Magnetic Field Laboratory, and the drive current was provided by an induction coil. This combination resulted in an EMAT that delivered 0.5 MPa (5 atmospheres) of acoustic drive to the surface of the sample while coupling less than 100 watts of incidental induction heating. In the initial experiment, aluminum samples of A356 alloy were heated to the liquid state and allowed to solidify at a controlled cooling rate while subjected to non-contact ultrasonic stimulation (at 165 kHz) provided by an induction coil located within the bore of the magnet.

RESULTS AND DISCUSSION

Aluminum samples processed ultrasonically with the high magnetic field EMAT were compared with samples processed without EMAT excitation (no-field), but with the same thermal treatment [1]. Based on visual appearance of the small ingots, samples processed with EMAT stimulation showed notably improved smoother surface conditions as compared with samples solidified without EMAT stimulation. Optical micrographs revealed obvious differences in microstructure. Micrographs for a no-EMAT sample exhibited an obvious variation in microstructure from the top to bottom of the ingot, suggesting segregation of Si, which is manifest in different amounts of primary alpha (~pure Al) versus eutectic (alpha plus Si-rich phase). By comparison, similar micrographs for a high-field EMAT processed sample showed no variations in microstructure uniformity.

CONCLUSIONS

A novel high-field EMAT has been developed and demonstrated as an effective non-contact ultrasonic processing methodology for application during the solidification processing of aluminum samples in a high field magnet.

ACKNOWLEDGEMENTS

We acknowledge Dr. Bruce Brandt and the staff at the National High Magnetic Field Laboratory for their support. Research sponsored by the Laboratory Directed Research and Development Program of Oak Ridge National Laboratory (ORNL), managed by UT-Battelle, LLC for the U. S. Department of Energy under Contract No. DE-AC05-00OR22725.

REFERENCES

[1] Wilgen, J.B, *et al*, "Non-Contact Ultrasonic Treatment of Metals in a Magnetic Field", in Materials Processing Under the Influence of External Fields, *Symposium Proceedings from the TMS 2007 Annual Meeting*, Orlando, FL, February 25-March 1, s2007, TMS Publishers, Warrendale, PA, 2007, **145**.

Pulsed magnets are the most advanced highly-stressed electro-mechanical systems presently in use; the energy-density of and power-flow into the magnetic field are comparable to a combustion chamber inside a rocket engine. The advance to 89 T reported here represents a major breakthrough of long standing barriers. This insert magnet is at the very center of the 100 T magnet objective. The achievement was possible because of the quality and performance of the design and novel state of the art materials developed to reliably reach these field intensities.

PERFORMANCE OF 1ST 90 T INSERT MAGNET FOR DOE-NSF 100 TESLA MULTI-SHOT MAGNET SYSTEM

C.A. Swenson (LANL, MPA-NHMFL), N. Harrison (LANL, MPA-NHMFL), J.B. Schillig (LANL, MPA-NHMFL), J. R. Sims (LANL, AET-1), and D.G. Rickel (LANL, MPA-NHMFL)

INTRODUCTION

The National High Magnetic Field Laboratories 100 T Multi-shot Magnet has completed phase one commissioning to deliver science at 85 Tesla. The US Department of Energy and the National Science Foundation supported the magnet system's development and construction. The magnet system is the culmination of 10 years of efforts by DOE and NSF design teams. The program goals for the first phase of operations are a non-destructive millisecond-scale 90 T pulse magnet system to support scientific research in high magnetic fields. Two magnet subsystems comprise the magnet: a nested array of seven generator-driven coils designed to produce ~ 40T in a 225 mm bore; and a capacitor-driven 15 mm bore "insert" magnet that developed to produce ~ 50 T inside the outer coil set. The US-DOE 100 T Multi-shot (MS) Pulsed Magnet Program is collaboration between US-DOE and US-NSF engineering teams at Los Alamos National Laboratory.

Technology for the 90 T insert evolved from a series of prototype magnets built to access engineering concepts and materials, and gain experience operating insert-like coils at the intensities encountered at 100 T. The insert magnet performance exceeded design specification by almost 15% delivering 53.6 T on a record system pulse of 88.9 T. The field measurement was made using a de Haas van Alphen measurement on pure copper. The magnet system enters the science user program providing the highest magnetic fields ever produced non-destructively.

Figure 1.
Insert magnet in transit to assembly inside 100 T outer magnet assembly

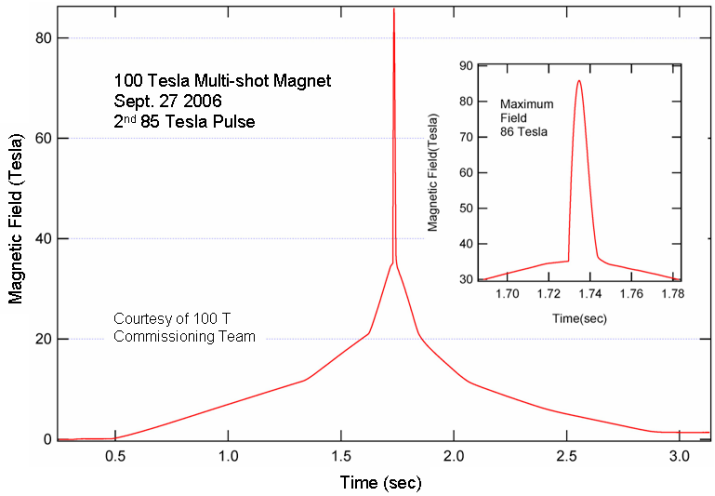

Figure 2.
Second 85 T pulse using insert and outsert magnet systems.

REFERENCES

[1] C.A. Swenson, *et al.*, Submitted to the proceedings of the Santa Fe Megagauss (2006).

The mouse brain image produced by the NHMFL is a very important advance, with a site (*http://nmr.magnet.fsu.edu/facilities/900Demos/MRIDemo.htm*) much visited. The advances described in this work continue to push resolution, important if, for example, MRI images are to be of comparable (and therefore comparable to) two-photon microscopy imaging. The technique reported here is fully functional and uses a three-element coil array that substantially improves signal/noise, and, hence response time and potentially, resolution.

FOCUSED PARALLEL IMAGING ARRAY FOR MOUSE BRAIN IMAGING AT 11.1T

B. Beck (UF, AMRIS), S. Grant (FSU, Chemical Engineering)

INTRODUCTION

In clinical settings, surface coil arrays offer high sensitivity and extended fields of view for human MRI that are crucial for diagnostic coverage. Coupled with parallel imaging (PI) techniques, these coil arrays dramatically decrease the acquisition times of clinical scans. However, for MR research efforts focused on *in vivo* animal models, the exact point of anatomical interest for imaging is often known *a priori* due to a predetermined disease or injury site. Array elements that are focused on a common location can provide the animal image with enhanced signal-to-noise performance, improved B1 field homogeneity at high magnetic fields and accelerated imaging times via PI methods. In this study, we present a receive-only array design for animal MRI at high fields (> 11 T) that focuses each element at a single location. Sample images were acquired at 11.1 T on biologically relevant phantoms and *in vivo* mice.

EXPERIMENTAL

A 3-element array was built on a curvilinear fiberglass half-shell of diameter 3.8 cm (Figure 1). The design consists of two orthogonal butterfly coils centered over a single loop coil. The single loop is 3.2 cm in diameter, built on a Teflon substrate, and has two distributed capacitors. The butterflies, also placed on the Teflon substrate, are 2.8 by 4 cm and have four distributed capacitors. Each coil element contains a passive trap (MA45471Schottky diodes) across one of the distributed capacitors. Small isolation capacitors are added between elements. The coil array was placed in a small transmit-only birdcage and parallel imaging was performed on a 11.1-T, 40-cm Magnex/Varian magnet interfaced with a Bruker Biospec imaging/ spectroscopy console and PI algorithms based on GRAPPA. The coil first was evaluated with a tissue equivalent phantom with characteristics of average brain at 470 MHz (ε =48.6, σ =0.6 S/m). *In vivo* brain imaging of a native C57 mouse followed. Fast Spin Echo (FSE) and Gradient-Recall Echo (GRE) images were acquired with acceleration factors of 2 and 3.

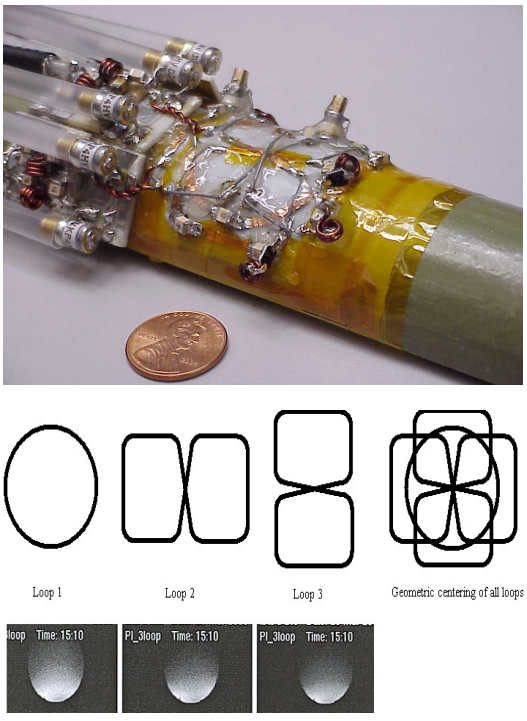

Figure 1.
Coil (left) and element profiles (right) showing focused coverage.

RESULTS AND DISCUSSION

Return loss for all coil elements was ≤ -22 dB, and isolation between all elements was better than 20 dB. The coil and axial profiles of each coil element, all focusing on the same volume, are shown in Figure 1. Figure 2 shows GRAPPA acquisitions of the *in vivo* mouse (with focal location in the cortex) with an acceleration factor of 2.

CONCLUSIONS

We have built, tested and utilized a 3-element surface coil array for mouse brain parallel imaging. Each element of the array is sensitive to the target region, thus maximizing the signal-to-noise in the volume of interest. GRAPPA images indicate good coverage and signal quality in the target volume of the mouse brain.

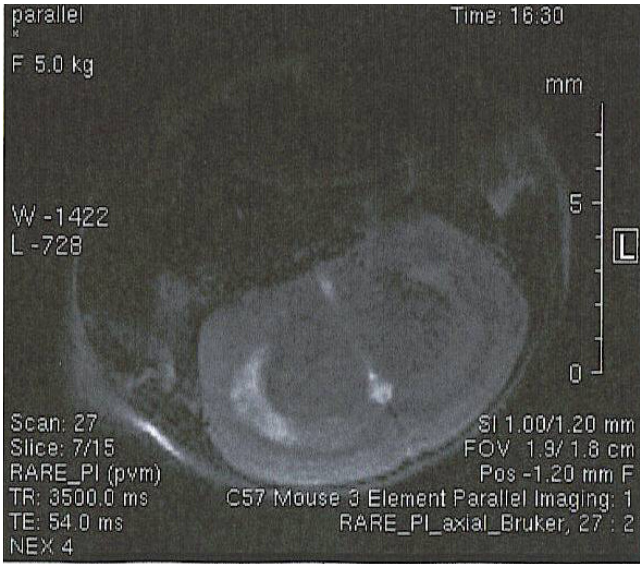

Figure 2.
Parallel Image of mouse brain.

ACKNOWLEDGEMENTS

Support was provided by NIH grant P41 RR 16105 and the National High Magnetic Field Laboratory.

REFERENCES

[1] B Beck *et al.*, accepted May 2007, ISMRM, Berlin 2007.

CONDENSED MATTER

KONDO/HEAVY FERMION SYSTEMS

For more than twenty years numerous efforts have been concentrated on understanding enigmatic properties of URu_2Si_2. URu_2Si_2 belongs to heavy fermions systems with a moderate mass enhancement. At T_N=17.5K the feature in its specific heat, C(T), reveals a sharp transition, most probably of the second order, into a new state the nature of which still remains unclear. Although the antiferromagnetic (AFM) ordering of the U-spins is confirmed in the neutron scattering experiments, the value of the staggered magnetization moments turns out so small ($\mu \sim 0.02\mu_B$) that the huge entropy loss at transition cannot be ascribed to their formation. Thus, a "hidden order" (HO) parameter of unknown symmetry and nature is hypothesized to account for the entropy changes at T_N.

Further NMR studies have revealed that staggered magnetization increases with applied pressure and reaches values reasonable for an AFM state. The dual interpretation of NMR results is possible. Thus, HO and AFM could coexist in space as sub-phases, and the AFM fraction increases with pressure for the account of the HO phase. Another option is that the order parameter *has two components whose relative weights change with pressure.*

In the report by Y.J. Lo *et al*. evidence is given in favor of this second point of view. The authors provide the (T,H)-phase diagrams for URu_2Si_2 at three different pressures. Their left hand sides correspond to HO/AFM: its shape varies insignificantly. Meanwhile, at the ambient pressure it is HO that is known to prevail, while with the pressure increase HO gets gradually "squeezed", and AFM begins to prevail. Inside, *i.e.*, at T below T_{HO}, changes in electronic properties take place with the field increase at some $T_p(H)<T_{HO}$. T_p itself marks a resistance maximum, but at lower T_p the Shubnikov-de Haas oscillations demonstrate that the increase in the Fermi surface (FS) size occurs at T_p. Abstracting from intermediate field-induced phases that become almost washed away with pressures, the rest of the phase diagram looks merely as a spin-flip transition from AFM into ferromagnetic phase (IV) in strong magnetic fields. No drastic changes are seen in HO/AFM part of the phase diagram with increase of pressure and magnetic field. It looks as a crossover between two components takes place from HO (at low pressure and fields) to AFM (localized spins).

This research was accepted for publication by **Physical Review Letters** *(in press) and was supported by the* **In-House Research program** (PI, Luis Balicas).

FIELD-INDUCED FERMI SURFACE RECONSTRUCTION AND ADIABATIC CONTINUITY BETWEEN ANTIFERROMAGNETISM AND HIDDEN-ORDER STATE IN URU_2SI_2

Y.J. Jo (NHMFL, CME); L. Balicas (NHMFL, CME); C. Capan (LSU, Physics) K. Behnia (EPSCI, Paris); P. Lejay (CRTBT, Grenoble); J. Flouquet (CEA, Grenoble); J.A. Mydosh (U. Cologne. I. Physics II); and P. Schlottmann; (FSU, Physics)

INTRODUCTION

The nature of the phase emerging at $T_0 \sim 17.5$ K which coexists with antiferromagnetism (AFM) in URu_2Si_2 remains elusive and has been called the ``hidden-order" (HO) state. None of the theoretical scenarios proposed can explain satisfactorily all the available data. In this Letter we present high field, low temperature electrical transport measurements in URu_2Si_2 under high hydrostatic pressure in order to gain insight on the interplay between the AFM and HO phases.

EXPERIMENTAL

We performed electrical transport measurement at very low temperatures by using the portable dilution fridge as well as hydrostatic pressure measurements using a ^{3}He insert in conjunction with the hybrid magnet [2].

RESULTS AND DISCUSSION

(a) The resulting *H-T* phase-diagram of URu_2Si_2 at p = 1 bar, shown for comparative purposes. The phase-boundary towards the HO state (phase I, following the nomenclature of Ref. [1]) is indicated by black dots. The position of a minimum in ρ within the HO-state is indicated by red circles. The position of the maximum observed in ρ within the HO state at T_ρ and where the geometry of the Fermi surface changes significantly is indicated by blue triangles. We nominate this new phase as phase I*. The boundary of the reentrant HO state (or phase III) is defined by magenta squares, while the boundaries of phases II and V are defined respectively, by orange circles and yellow triangles. The recovery of a FL state at T_{FL} is indicated by red crosses. Finally, the crossover from positive to negative magnetoresistance within the higher temperature metallic state is indicated by blue crosses. (b) Same as in (a) but under a pressure p = 8 ± 1 kbar. (c) Same as in (a) but for a pressure p = 11 ± 1 kbar.

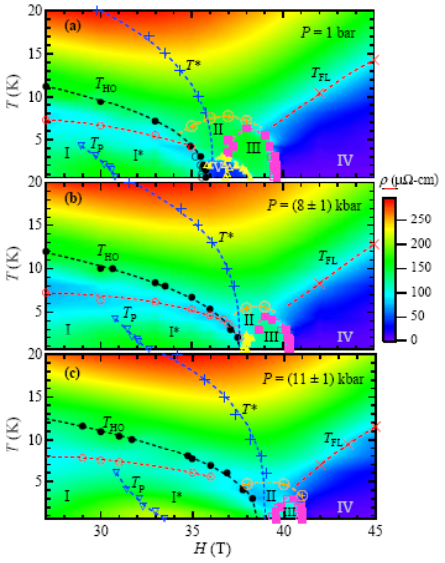

CONCLUSIONS

Our observations favor a scenario where the evolution from HO to AFM under pressure is a crossover rather than a phase transition with two competing coupled order parameters in the mixed phase, i.e., an adiabatic continuity between HO and AFM with gradual change in their weight with field and pressure. The picture of the HO-state emerging from this study indicates a semi-metallic state containing an intrinsic dipolar component which has Fermi surface pockets enclosing a volume of ~ 1.5 % of the Brillouin zone. It becomes slightly more metallic (in agreement with the Hall effect) under field, as indicated from the increased Fermi surface cross-sections in the SdH oscillations at T_ρ, then into a sequence of field-induced phases (which are shifted to higher fields and lower temperatures under pressure), and finally into the metallic FL phase IV. This increase in the density of carriers and the coexistence between HO and AFM is difficult to reconcile with a purely local crystalline field picture. Pressure increases the direct overlap between 5*f*-orbitals of nearest neighbor U-ions. This should favor an AFM phase.

ACKNOWLEDGEMENTS

YJJ acknowledges the NHMFL Schuller postdoctoral program while LB acknowledges support the NHMFL in-house research program.

REFERENCES

[1] Jo, Y.J., *et al.*, Phys. Rev. Lett. (in press)

CONDENSED MATTER

SUPERCONDUCTIVITY—BASIC

Experimental efforts in studying puzzling properties of the so called pseudogap (PG) state for the high temperature (HT_c) superconducting cuprates continue. Besides that the mechanisms of the HT_c superconductivity in cuprates remain unknown, experimental facts show that even the very transition between normal and superconducting states is unusual there. Thus, large diamagnetism is seen by different means in $La_{2-x}Sr_xCuO_4$(LSCO) and other HT_c cuprates, at temperatures that may exceed T_c even by a factor of four. These facts have led to suggestions that condensation of electrons into the Cooper pairs, which in ordinary SCs takes place directly at T_c, in cuprates bears a two-stage character. Namely, initially a formation of incoherent pairs takes place; the *phase coherence* between the latter sets in only with the further temperature decrease down to the SC onset at T_c.

The Princeton group (N.P. Ong) first reported observations of diamagnetism via the Nernst effect studies. The effect, known to be extremely small in metals, turned out to be strong for cuprates at temperatures larger than T_c. This has been ascribed to formation of vortices *above* T_c in strong enough magnetic field on a SC background: the Nernst effect would come about from the vortices' motion perpendicular to the thermal flow. The vortices were also seen in the magnetization experiments.

In the report by Lu Li *et al*. these ideas were further extended. The authors studied low doped LSCO at low temperatures, at x below the optimal doping and, most extensively, in the vicinity of the threshold concentration, x_c=0.055, below which SC was not seen as the bulk phenomenon. Using the magnetometry technique, the phase diagram in the (x, H)-plane was constructed at low enough temperatures. Boundaries between vortex liquid and vortex solid have been measured. The bottom line is that vortices become formed in the presence of applied magnetic field even at $x<x_c$, thus manifesting some incoherent SC background in this strongly underdoped regime. In particular, the critical field, H_{c2} is finite at $x \mapsto 0$. Experiments display peculiarities of the Berezinskii-Kosterlitz-Thouless transition in layered cuprates.

This research is to be published in **Nature Physics** *2007.*

LOW TEMPERATURE VORTEX LIQUID IN SINGLE-LAYERED HIGH T_C CUPRATES

L. Li, Y. Wang, J. G. Checkelsky, N. P. Ong (Princeton Univ., Physics); S. Komiya, S. Ono, Y. Ando (CRIEPI, Tokyo)

INTRODUCTION

High resolution torque magnetometry is a unique method for measuring magnetization in intense field of high T_c cuprates. These measurements uncover diamagnetism above T_c and display unconventional T dependence of H_{c2}. H_{c2} is finite at T_c and remains almost independent of T for $T < T_c$[1,2,3]. An interesting question is how H_{c2} evolves in the phase diagram, especially as superconductivity disappears as the doping x decreases below the critical doping $x_c = 0.055$. Lightly doped LSCO ($0.03 \le x \le 0.09$) single crystals are measured by using torque magnetometry down to pumped He^3 temperature 0.35 K.[4]

EXPERIMENTAL

Detailed torque magnetometry measurements are carried out in a 33 T resistive DC magnet (cell 9) with a user provided vacuum sealed He^4 probe and in the 31 T 50 mm bore magnet (cell 5) with the He^3 insert at the NHMFL.

RESULTS AND DISCUSSION

The top panel at right displays typical magnetization curves for the measured lightly doped LSCO. Though not superconducting, magnetization curves show a negative "dip" at low field 0 – 10 T, which suggests diamagnetism arising from the vortex liquid state. At higher fields, magnetization tends to saturate, showing the contribution of paramagnetic anisotropic spins. The net result is an interesting oscillating behavior which occurs at 0.5K and 0.75K. After separating the aforementioned paramagnetic contribution, the diamagnetic signal with characteristic "tilted-hill" feature is restored and we are able to determine H_{c2}. The phase diagram in the right panel shows H_{c2} at the lowest achievable temperature 0.35K for different dopings. H_{c2} extends smoothly across the critical doping $x_c = 0.055$. Blue shading displays the region of spin anisotropy contributing to magnetization. We also measure irreversible MH behavior and detect the field H_{irr} where this hysteresis stops. Since MH hysteresis arises from pinning in the vortex solid state, H_{irr} provides a good probe to study the melting of the vortex solid and additionally approaches the real melting field at the lowest temperatures.

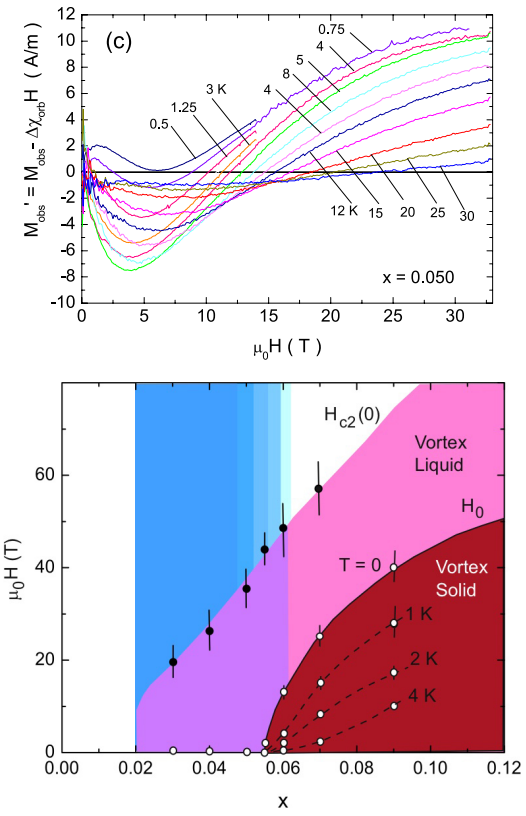

Figure 1.
Top panel: Curves of magnetization M vs. field H up to 32 T in the $La_{2-x}Sr_xCuO_4$ (x = 0.050) at select T; Bottom panel: x-H phase diagram at low temperature showing vortex liquid and vortex solid state [4] .

CONCLUSIONS

Diamagnetic signals of vortices are observed in lightly doped LSCO, even for doping x below the critical doping $x_c = 0.055$. Doping and temperature dependence are studied with torque magnetometry for two field scales, the upper critical field H_{c2} and the melting field H_{irr}. The results suggest that below x_c, the pair condensate survives as a vortex liquid, though long range phase correlation is absent down to 0.35K.

ACKNOWLEDGEMENTS

This work is supported by a NSF grant (DMR 0213706). The authors wish to thank Dr. Scott Hannahs, Dr. Alexei Souslov and Dr. Eun Sang Choi for their generous assistance during the experiment.

REFERENCES

[1] Yayu Wang, Lu Li *et al.*, Phys. Rev. Lett., **95**, 247002 (2005).
[2] Lu Li, *et al.*, Europhys. Lett., **72**, 451 (2005).
[3] Yayu Wang, Lu Li, N.P.Ong , Phys. Rev. B., **73**,024510 (2005)
[4] Lu Li *et al*,. Nature Physics 2007, in press. DOI: 10.1038/nphys563

MAGNETISM AND MAGNETIC MATERIALS

The report by V. R. Fanelli *et al*. deals with the magnetic properties of Pr_3In. The Pr-ion in Pr_3In has a singlet as the ground state. The antiferromagnetic transition at T_N=11.4K is, therefore, due to a weak admixture of the low-lying triplet caused by the exchange interactions between Pr-ions on neighboring sites. The authors investigate the spin-flip transition, i.e., polarization of spins in large magnetic fields. Rather small energy distance between Crystal Field singlet and triplet levels (~6.3 meV) makes possible strong sensitivity of the staggered moments to applied field and other effects that are not fully resolved yet.

This research was supported by the **In-House Research Program** (PI, Marcelo Jaime).

The interest persists in properties of multi-ferroics caused also by potential applications. Symmetry of these materials allows coupling between ferroelectric and magnetic parameters that can be tuned by magnetic fields.

In the report by J.W. Kim *et al*. the magnetic field induced transition is found in $BiMn_2O_5$ with the quantum critical point (QCP) at the critical field 18T providing an example of a ferroelectric QCP. The transition manifests itself also in a spike-like feature for the dielectric constant.

R.C. Rai *et al.* discovered significant high energy magneto-dielectric effects (changes in the dielectric constant with applied magnetic field) in the S = 1 Kagome staircase material Ni3V2O8. Here, magnetic frustration and spin-lattice-charge coupling gives rise to a complex H-T phase diagram, the optical properties of which were carefully investigated by the authors. $Ni_3V_2O_8$ is an intermediate gap, local moment band insulator with electronic structure that is particularly favorable for magneto-dielectric coupling. The high energy magneto-dielectric contrast is as large as 16% near 1.29 eV, and it can be positive or negative depending on the energy. This work is reported in Physical Review B **74**, 235101 (2006) and is supported by the DoE.

This work is reported in **Physical Review B, 74**, 235101 (2006).

HIGH FIELD MAGNETIZATION IN THE INDUCED MAGNETIC MOMENT SYSTEM PR_3IN

V.R. Fanelli (UC Irvine, Physics and MPA-NHMFL), M. Jaime (MPA-NHMFL), J. Thompson (MPA-NHMFL), J.M. Lawrence (UC Irvine, Physics), A.D. Christianson (ORNL), N. Harrison (MPA-NHMFL), H.S. Suzuki (Nat. Inst. for Mat. Science, Tsukuba, Japan)

Pr_3In is a compound showing induced moment magnetism in a singlet-triplet system. Neutron diffraction, magnetic susceptibility and specific heat measurements reported by Christianson *et al*. [1] show that Pr_3In exhibits induced moment antiferromagnetic (AF) order with T_N=11.4K. Previous specific heat (C_p) measurements performed at NHMFL-LANL show that the magnetic field causes a strong reduction of C_p and also reduces T_N while magneto-caloric effect (MCE) indicates a phase transition occurs at 1.9 T, below 11K.

In this system, the exchange interaction between Pr sites causes admixture between crystal field levels (inset, Fig.1b) resulting in induced moment magnetic order below T_N. Application of a magnetic field can change the energies of the singlet and triplet in such a manner as to alter the admixture. At high enough fields there should be a transition from the AF phase to a FM-aligned (polarized) phase. At present, we do not know whether the phase above 1.9 T involves a spin rearrangement, e.g. a spin flop, or whether it is a spin polarized phase. It would be surprising for it to be to a spin polarized state in that for T_N =11.4 K, we expect such a transition to take place at values of magnetic field greater than 10 T. In measurements of magneto-caloric effect to 15 T at NHMFL-LANL, we have not observed a second phase boundary for B < 15 T. Our motivation for studying the magnetization was to explore if there is another transition between 20 and 50 T, and to

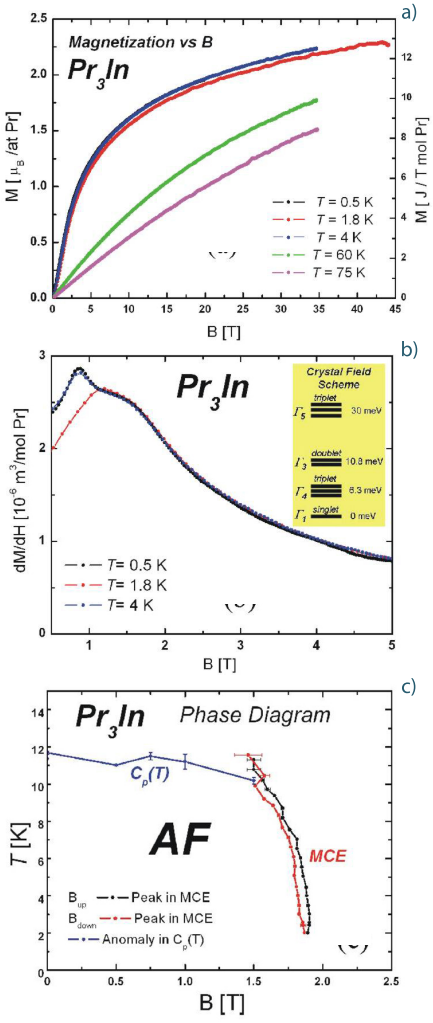

Figure 1.
a) Magnetization versus magnetic field at 0.5 K, 1.8 K, 4 K, 60 K and 75 K. b) Mass Susceptibility (dM/dH) for T=0.5K, 1.8K and 4K. Inset: relevant crystal field scheme. c) Phase diagram determined through the anomalies in C_p/T, peaks in temperature in MCE for both increasing and decreasing B.

find the saturation field B_{sat} for the high-field phase in order to obtain the energy-scale for the exchange interaction between Pr sites.

Magnetization as a function of magnetic field was measured using the 50T pulsed magnet at NHMFL-LANL. No anomaly corresponding to a phase transition was observed in the range 2<B<45 T, raising the possibility that the 1.9 T transition does indeed involve ferromagnetic polarization. For T< 4 K, the magnetization was observed to saturate at a field of order of 50T, consistent with the energy required to completely polarize the Γ4 triplet at 6.3 meV. The mass susceptibility (dM/dH) shows two features: one around 1 T and another at 1.5 T. The second one is consistent with the transition observed through MCE (Fig. 1c). Since the first one does not show up consistently for all temperatures, it is likely an artifact originated in the time integration of the raw data.

ACKNOWLEDGEMENTS

This work was performed at NHMFL-LANL, and supported by US DOE Grant No. DE-FG03-03ER46036, by NSF Cooperative Agreement No. DMR-0084173 by the State of Florida and US DOE, and partially supported by NHMFL IHRP.

REFERENCES

[1] Christianson, A.D., *et al*., Phys. Rev. B **72** (2005) 024402.

MAGNETIC-FIELD-INDUCED QUANTUM PHASE TRANSITITON IN $BIMN_2O_5$

J. W. Kim, S. Y. Ham, Kee Hoon Kim (Seoul National University, Physics & Astronomy); S. Park, S.-W. Cheong (Rutgers University, Physics & Astronomy); M. Jaime (LANL-NHMFL)

In our previous investigations of magnetic field-temperature phase diagram of multiferroic RMn_2O_5 (R= Tb, Dy, Y, and Bi) compounds [1], we have discovered a common phase boundary with similar shape at high field (>18 T) for all compounds. Particularly for $BiMn_2O_5$, polarization (*P*) change from low field positive to high field negative at the phase boundary. Interestingly, a large peak in dielectric constant (ε) is found at the zero polarization state. This magnetic-field-induced ferroelectric transition has been studied in detail by dielectric constant, electric polarization, magnetization and heat capacity measurements.

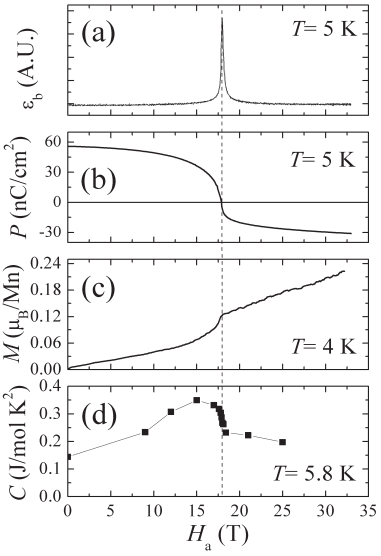

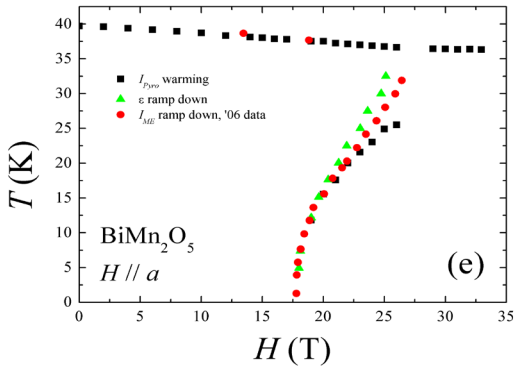

Figure 1.
(Left panel) Magnetic field dependent (a) dielectric constant, (b) electric polarization, (c) magnetization and (d) heat capacity at fixed temperatures. (Right panel) (e) Magnetic field-temperature phase diagram of $BiMn_2O_5$. A single magnetic field induced transition exists down to 0.6 K.

A home-made transport stick with 12 coaxial wires and 18 phosphor-bronze wires is used for ε and *P* measurements. Heat capacity is measured with a Si-based heat capacity probe. Magnetization is measured with a compensated coil susceptometer adapted for use in a pulse magnet at LANL-NHMFL. All other measurements are done in a DC resistive magnet in NHMFL, Tallahassee. The electric contacts were made in the *b*-plane and magnetic field is applied along the *a*-axis of the sample.

Fig. 1 (a)-(d) shows the magnetic field dependent dielectric constant, polarization, magnetization, and heat capacity of $BiMn_2O_5$, respectively. The dielectric constant shows a sharp peak at the critical field ~ 18 T. Polarization changes sign from positive to negative, and magnetization shows a sharp increase near the critical field. With increasing field, heat capacity increases up to ~ 15 T. After a maximum value at 15 T, heat capacity decreases steeply near the critical field and decreases slowly up to 25 T. Magnetic field-temperature phase diagram of $BiMn_2O_5$ is plotted in (e). The trajectory of the phase boundary at high field follows the scaling relation $T_c(H) \sim (H-H_c)^{1/2}$, which is similarly found in quantum paraelectrics or incipient ferroelectrics such as $KTaO_3$ and $SrTiO_3$ [2].

These observations support an interesting possibility that $BiMn_2O_5$ can be the first system to exhibit quantum fluctuation of ferroelectricity tuned by magnetic field.

ACKNOWLEDGEMENTS

This work is supported by the National Research Laboratory program (M10600000238) by the Korean Ministry of Science and Technology. The work at NHMFL is performed under the auspices of the National Science Foundation, the State of Florida, and the U.S. Department of Energy.

REFERENCES

[1] S. Y. Haam *et al.*, Ferroelectrics **336**, 153-159 (2006); J. W. Kim et al. to be submitted.
[2] W. R. Abel, Phys. Rev. B **4** (1971) 2696; K. A. Muller and H. Buckard, Phys. Rev. B **19** (1979) 3593.

DISCOVERY OF HIGH-ENERGY MAGNETO-DIELECTRIC EFFECT IN A FRUSTRATED KAGOME LATTICE MATERIAL

R.C. Rai, J. Cao, S. Brown, J.L. Musfeldt (U. Tennessee, Chemistry); D. Kasinathan (UC Davis); D.J. Singh (ORNL); G. Lawes (Wayne State); N. Rogado, R.J. Cava (Princeton); X. Wei (NHMFL)

INTRODUCTION

$Ni_3V_2O_8$ has attracted attention as a potential high energy magnetodielectric material due to strong spin-lattice coupling, unusual frustration effects, and a complex phase diagram. The ferroelectric phase is particularly interesting because it has coupled magnetic and electric domains. We used a combination of optical spectroscopy, first principles calculations, and energy dependent magneto-optical measurements to elucidate the electronic structure and to study the phase diagram of $Ni_3V_2O_8$. The high energy magneto-dielectric contrast is as large as 16% at 1.29 eV.

RESULTS AND DISCUSSION

The magneto-optical response of $Ni_3V_2O_8$ is very rich, with a remarkable interplay revealing additional high magnetic field phases and an unexpected electronic structure which we associate with the strong magneto-dielectric couplings in this material over a wide energy range. Specifically, we observed several prominent magneto-dielectric effects that derive from changes in crystal field environment around Ni spine and cross-tie centers. This effect is consistent with a field-induced modification of local structure. Symmetry-breaking effects are also evident with temperature. We find $Ni_3V_2O_8$ to be an intermediate gap, local moment band insulator. This electronic structure is particularly favorable for magneto-dielectric couplings, because the material is not subject to the spin charge

separation characteristic of strongly correlated large gap Mott insulators, while at the same time remaining a magnetic insulator independent of the particular spin order and temperature.

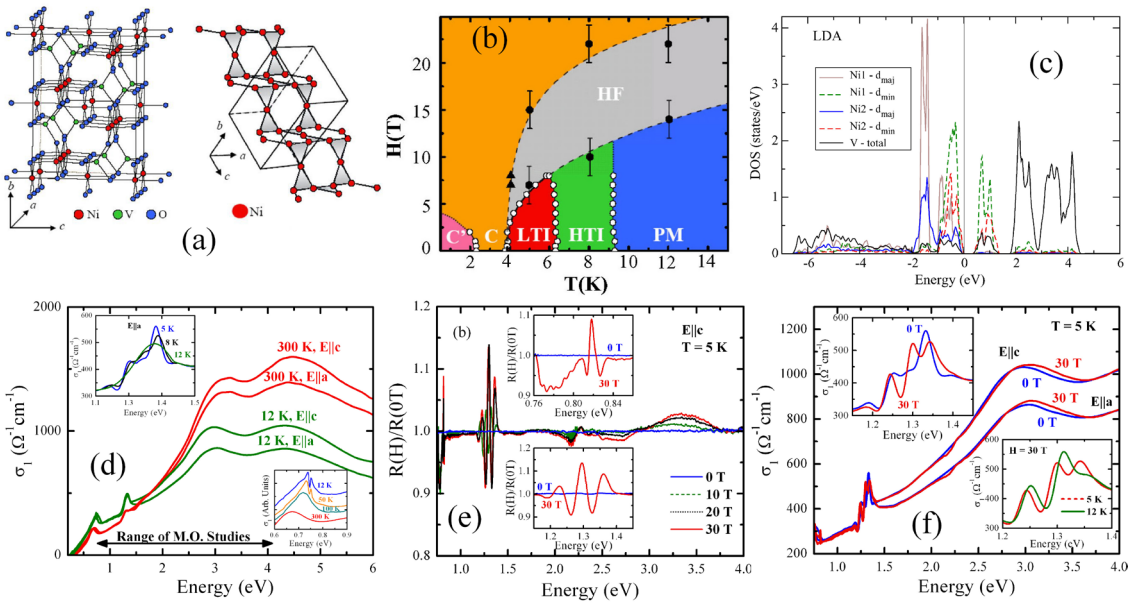

Figure 1:
(a) Crystal structure of $Ni_3V_2O_8$, (b) H-T phase diagram, (c) calculated density of states, (d) variable temperature optical conductivity, (e) magneto-optical reflectance, and (f) optical conductivity in high magnetic field. Note the field-induced splitting of the Ni (spine) d to d on-site excitation (insets, panel (e)).

ACKNOWLEDGEMENTS

We thank the U.S. Department of Energy for support of this work.

OTHER CONDENSED MATTER

Properties of a number of materials with significant potential applications are being studied at NHMFL facilities.

J. Shaver *et al*. investigated the excitonic structure of single-walled carbon nanotubes through photoluminescence excitation spectroscopy. They utilized the Aharonov-Bohm effect to modify the excitonic transitions such to "brighten" an optically inactive state. The high fields available at the Magnet lab allow this team to observe the signature of this optically inactive, "dark exciton" as an increase in photoluminescence intensity at low temperatures and two peaks in spectra at high temperatures.

This research was supported by the **In-House Research Program** (PI, David Reitze).

P. D. Ye *et al*. report preliminary studies on possible applications of the carbon nano-tubes in the area of field-effect transistors.

The report by S.N. Sprunt et al. describes the study of liquid crystals (the systems that have extremely wide technological applications) that relied on birefringence produced in high magnetic fields to obtain the signature of a new state of matter—the tetrahedratic phase with the third-rank tensor as the order parameter.

This research has been submitted to **Phys. Rev. Lett.**

CONDENSED MATTER

MAGNETO-PHOTOLUMINESCENCE SPECTROSCOPY OF CARBON NANOTUBES

J. Shaver, S. Zaric, T. Searles, J. Kono (Rice U., ECE); Y. D. Jho, X. Wei (NHMFL); R. H. Hauge (Rice U., Chemistry), V. Perebeinos (IBM), Y. Miyauchi, S. Maruyama (U. Tokyo, Mech E.)

Recent theory [1-4] has predicted the existence of optically-inactive, or "dark" excitons in single-walled carbon nanotubes (SWNTs) *below* the first optically-active, or "bright" exciton state. This could trap much of the exciton population and contribute to the low quantum yield. Dark states arise due to the doubly-degenerate conduction and valence bands of SWNTs as well as the characteristic strong Coulomb interactions among charge carriers in low-dimensional systems.

We have measured near-infrared polarized photoluminescence (PL) on micelle-suspended SWNT samples in magnetic fields up to 45 T at room temperature (Fig. 1a) and PL excitation on an aligned gelatin SWNT film at low temperature up to 35 T (Fig. 1b). PL measurements were performed using the 45 T Hybrid Magnet, while PL excitation (PLE) was done in a 35 T resistive magnet.

We demonstrate that a magnetic field can significantly increase the PL of semiconducting SWNTs by "brightening" the dark exciton state. At low temperature, the PL intensity increased, or "brightened", with magnetic field. At high temperature, the PL peaks split into two peaks, the amount of which was proportional to the amount of flux threading the tube.

A magnetic field applied to the tube axis removes the valley degeneracy by lifting the time-reversal symmetry producing two equally-bright excitonic states at high magnetic fields [5,6]. This degeneracy lifting mixes different parity excitonic wave functions providing excitons trapped in the dark state with a radiative recombination pathway, thus brightening the transition. At low temperatures, this is manifest as an increase in PL intensity due to the exciton population being trapped in the lower, dark state, as well as a red shift proportional to the applied field. At high temperature, there is a finite population in the upper, bright state before the field is applied resulting in a two split peaks once the symmetry is broken by a magnetic field. This work clearly demonstrates the existence of dark excitons in SWNTs.

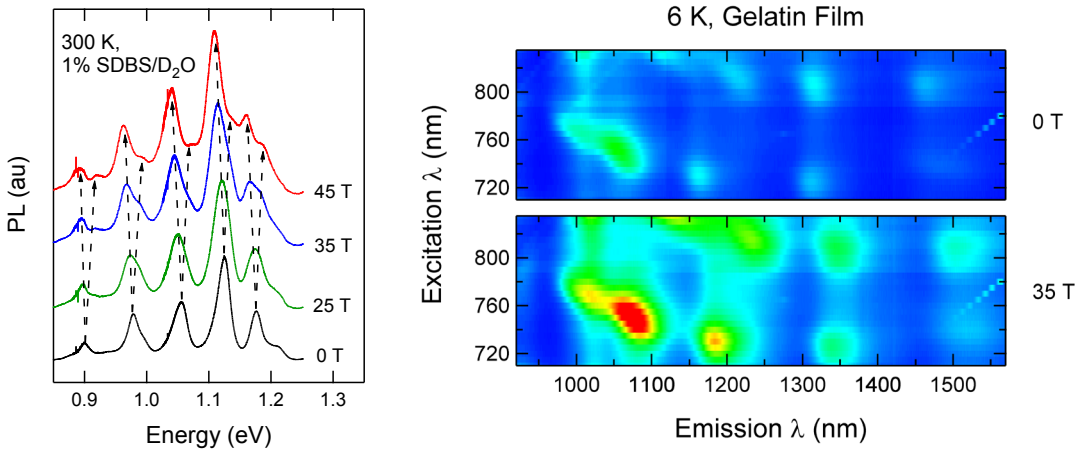

Figure. 1
Magneto-PL data: (a) 725nm excitation light polarized parallel to *B* measured at the fields shown at room temperature for liquid SWNT suspension. Peaks are split by an amount proportional to the applied field. (b) PLE data taken at 0 T and 35 T at 6 K. PL intensity increases with field as peak position red shifts.

REFERENCES

[1] Perebeinos, V., *et al.*, Phys. Rev. Lett. **92** (2004) 257402.
[2] Zhao, H., Mazumdar, S., Phys. Rev. Lett. **93** (2004) 157402.
[3] Perebeinos, V., *et al.*, Nano Lett. **5** (2005) 2495-2499.
[4] Ando, T., J. Phys. Soc. Jpn. **75** (2006) 024707.
[5] Zaric, S., *et al.*, Phys. Rev. Lett. **96** (2006) 016406.
[6] Shaver, J., *et al.* Cond-Mat/0702036

MICROWAVE PHOTORESISTANCE SPECTROSCOPY OF SINGLE-WALLED CARBON NANOTUBES

P.D. Ye (Purdue U., Electrical Engineering), L.W. Engel (NHMFL), S.K. Kim, S. Mohammadi (Purdue U., Electrical Engineering), C.J. Wang, M.S. Shim (UIUC, Material Science and Engineering)

INTRODUCTION

Since their discovery in 1991, carbon nanotubes (CNTs) have been the focus of intensive research for many potential applications, including sensing, textile, chemistry, biology and electronics, to name a few. CNTs are rolled up sheets of graphitic carbon with minimum diameter of 1.2 nm and are available in single-walled and multi-walled forms. Because of its perfect one-dimensional crystalline structure, CNTs exhibit unusual physical, chemical and mechanical properties, i.e., the exotic Luttinger liquid behavior in electrical transport properties. Recently, there has been tremendous interest in using CNTs as channels of field-effect-transistors (FETs) since these have the potential to replace the Si CMOS technology in microelectronic industry. The RF response is of great importance to evaluate this novel nano-device. But it is very challenging to characterize the RF performance of CNT transistors since the impedance of CNTs is mismatched with the standard 50 Ω input of RF instrumentation, hence the present, initial investigation looks at photoresistance of the CNT device under microwave radiation.

EXPERIMENTS

We have successfully developed a novel CNT-FET with a poly-Si bottom gate structure. The device has a gate length of 1 μm and achieves a unity gain frequency f_T of 2.5 GHz and a maximum oscillation frequency f_{max} of > 5 GHz. In this microwave photo-response experiment, we study the quasi-dc electrical transport properties of both metallic and semiconducting single-walled CNTs under high-frequency (RF and microwave) excitations at dilution refrigerator temperatures using NHMFL microwave capability.

RESULTS AND DISCUSSION

Figure 1(a) summarizes our findings on quasi-metallic single-walled CNTs under microwave radiation. The resistance of CNT at B=0 is almost at constant value of 300 KΩ independent on microwave radiation from 50 MHz up to 20 GHz. A negative resistance peak emerges at 5 GHz when B field is a fraction of 1 Tesla and becomes more pronounced with the increase of B field. The $\Delta R/R_0$ is about 5% as B field reaches 18 T. Possible harmonic features are also observable, for example around 10 GHz. The effect becomes more pronounced on increasing microwave power as shown in Fig. 1(b). No resonances were observed in semiconducting CNTs with the same device and measurement configuration. Figure 1(c) shows the impedance-matching equivalent circuit for CNT sample, which explains all the experimental observation. More experiments and theoretical studies are needed to clarify the origin of the sensitivity of the device to microwave radiation.

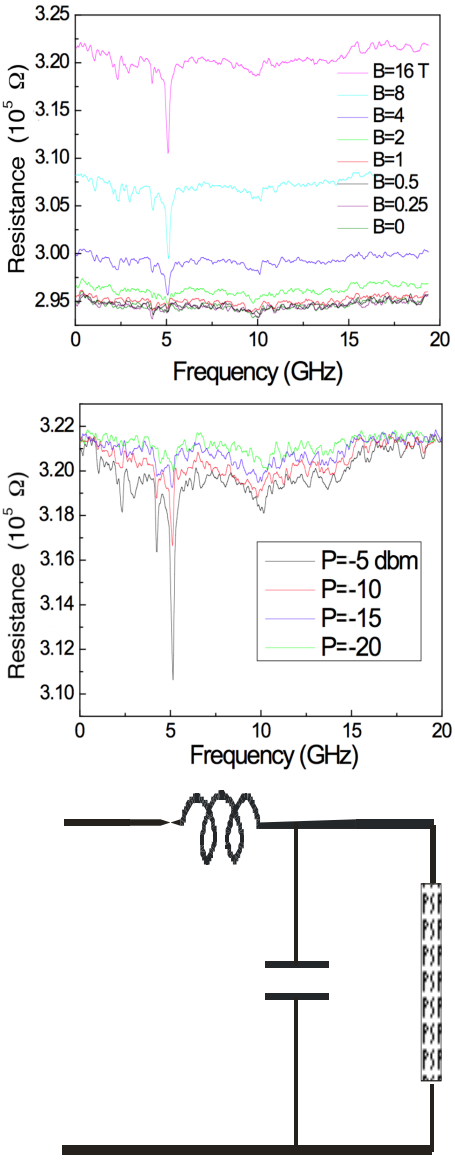

Figure 1.
Single walled CNT under microwave radiation resistance vs microwave frequency (a) at various magnetic fields. and -5 dBm applied at top of cryostat b) at 16 T for various power levels, in dBm at top of cryostat. Only a small fraction of the power applied couples into the sample, which was in mixture at a temperature of about 60 mK. (c) equivalent circuit for the resonator model to explain the experimental results.

HIGH-FIELD MAGNETO-OPTICAL STUDIES OF LIQUID CRYSTALS AND COMPLEX FLUIDS

S.N. Sprunt, J.T. Gleeson, A. Jakli, D. Wiant, K. Neupane (Kent State University)

INTRODUCTION

Bent core nematic liquid crystals bring exciting opportunities for both new technological applications and fundamental science. Concerning the latter, one important prediction is the existence of a new state of matter, comprised of such liquid crystals which are tetrahedratically ordered. That is, has the orientational symmetry of a tetrahedron, described by a third-rank tensor order parameter. This state will be particularly difficult to identify because it will be optically isotropic, and therefore not detectable via usual techniques. Our approach was to search for this substance using magnetic field induced optical birefringence. Preliminary experiments at KSU showed promising indications, but we could not produce sufficiently intense fields to make definitive conclusions.

EXPERIMENTAL

We therefore built a custom built oven and stage designed for Cell 4 in Tallahassee. This apparatus folded a laser beam from an optical breadboard on the floor beneath the bore, up to the oven which was held at the bore center, then transverse through the liquid crystal (so that the beam traveled perpendicular to the field) and then back down to the optical breadboard for analysis. These measurements were obtained as functions of both temperature and magnetic field (up to 19T) during May, 2006. A photograph of our oven and tower assembly is at right.

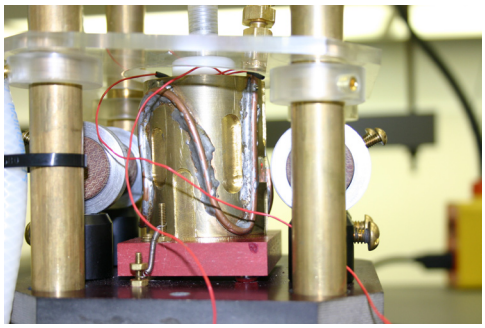

RESULTS AND DISCUSSION

Our high magnetic field results, when taken in conjunction with independent dynamic light scattering and high resolution calorimetry studies, demonstrate convincingly, for the first time, the existence of the tetrahedratic phase. Example data is shown at right; traditional liquid crystals will exhibit a constant Cotton-Mouton coefficient (i.e. a straight line through the origin). The example clearly indicates non-linear behavior, which is a signature of the tetrahedratic phase.[1] Such data could only be obtained using the non-conventional magnetic field capabilities of NHMFL.

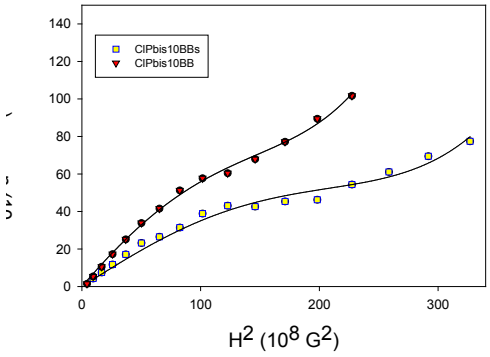

ACKNOWLEDGEMENTS

This work has been supported by the National Science Foundation (NSF-DMR-0606160) and Kent State University.

REFERENCES

[1] Wiant, D.B. *et al*, "Observation of a possible tetrahedratic phase in bent-core liquid crystals", submitted to Physical Review Letters, April, 2007.

CONDENSED MATTER

METAL-INSULATOR TRANSITIONS

The report by J. Huang *et al*. describes transport studies performed on an ultra-clean two dimensional electron gas, at temperatures lower then those ever studied so far. This study is interesting, because the low temperature transport at such low electron densities is believed to be dominated by strong electron-electron interaction, where conventional theory most likely does not apply. Indeed, the experiments observe an insulating-like temperature dependence of the resistivity at the lowest temperatures, which nevertheless seem to saturate to a finite resistance at T=0. This behavior seems at odds with theoretical expectations, and will stimulate further theoretical and experimental work.

DISAPPEARANCE OF THE METAL-LIKE BEHAVIOR IN GaAs TWO-DIMENSIONAL HOLES BELOW T=30 MK

J. Huang (Princeton University); J.S. Xia (NHMFL, High B/T Facility); D. C. Tsui (Princeton University); L.N. Pfeiffer (Bell Labs); K.W. West (Bell Labs)

INTRODUCTION

The discovery of the metal-insulator transition (MIT) in two-dimensional (2D) systems bears fundamental importance towards the understanding the electron-electron interaction effects. The experimental studies have proven to be challenging because the usual disorder present in the system is large enough to overwhelm the Coulomb effects so that the charges are localized. Thus, a clean 2D environment is desired. Despite the large amount of evidence of MIT, there remains a central question on whether the metal-like behavior, observed at finite temperatures *(T)* as low as 30 mK, will survive at even lower *T*. Performing ultra-low *T*-dependence measurement, which demands effective cooling of 2D charges, is therefore essential.

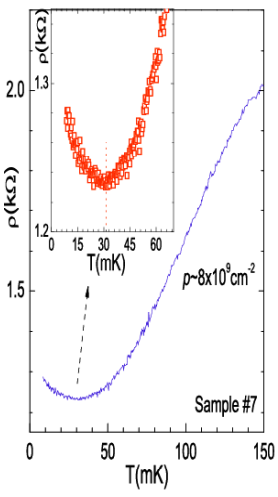

Figure 1.
ρ(T) for p=8x10^{9}cm^{-2}.

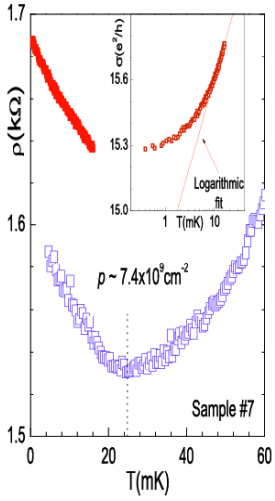

Figure 2.
ρ(T) for p=7.4x10^{9}cm^{-2}.

EXPERIMENTAL

We adopt a clean 2D-hole system in a novel *GaAs/AlGaAs* heterojunction insulated-gate field-effect transistor (HIGFET). Without any intentional doping, the device demonstrates exceptional mobility and density tunability (down to 5x10^{8}cm^{-2}). New observations have recently been made in such devices [1,2]. In this work, by utilizing the remarkable cooling techniques developed by Xia *et al.* [3] (who demonstrated a cooling of 2D electrons down to 4 mK), We have performed charge transport measurements on a very high quality p-channel HIGFET device in a nuclear demagnetization refrigerator at the Microcalvin lab at University of Florida, with an ultra-low temperature sweep down to a minimum liquid ^{3}He bath temperature of 0.5 mK.

RESULTS AND DISCUSSION

The *T*-dependence of the resistivity ρ for two different charge densities *(p)* is shown in Fig.1 and 2. Remarkably, for p=8x10^{9}cm^{-2} [Fig.1], following the metal-like behavior *(dρ/dT>0)* occurring at

higher *T*, ρ reaches a minimum around 32mK and rises from 1.22 kΩ to 1.29 kΩ with cooling down to ~9mK, signifying a crossover into an insulator-like regime *(dρ/dT<0)*. The inset is a blow-up of ρ at low-*T*. The same behavior is observed for p=7.4x10^{9}cm^{-2} which corresponds an rs value of 33 [Fig.2]. Notice that the curve in red, obtained after the demagnetization, corresponds to a slightly different density than before. Now, ρ reaches its minimum at a lower *T* of 25 mK, then rises with cooling down to a base *T* of 0.5 mK. The red curve shows an increase of ρ from 1.63 kΩ at 16mK to 1.69 kΩ at 0.5mK. The inset indicates thatthe transport is different than the weak-localization correction.

CONCLUSIONS

For a fixed carrier density around for p=8x10^{9}cm^{-2} for which only the metal-like behavior is anticipated, we have observed a crossover from the metal-like state *(dρ/dT>0)* into an insulator-like state when *T* is lowered below ~30 mK, and this insulator-like behavior *(dρ/dT<0)* prevails down to the lowest bath *T* of 0.5 mK. Despite the possibility of heating, the rising of ρ indicates that the charges are definitely being cooled. This qualitative change, occurring for resistivity much less than the quantum resistance, suggests that the metal-like behavior is likely a finite temperature effect and the ground state is possibly insulating.

ACKNOWLEDGEMENTS

The work at Princeton Univ. is funded by a US NSF MRSEC grant DMR-0213706 and DOE grant DEFG02-98ER45683.

REFERENCES

[1] Jian Huang, D. S. Novikov, D. C. Tsui, L. N. Pfeiffer, and K. W. West, Phys. Rev. B **74**, 201302(R) (2006)
[2] Jian Huang, D. S. Novikov, D. C. Tsui, L. N. Pfeiffer, and K. W. West, cond-mat/0610320 (2006, submitted to PRL)
[3] J. S. Xia, E. D. Adams, V. Shvarts, W. Pan, H. L. Stormer and D. C. Tsui, Physica B **280**, 491 (2000, submitted to PRL)

MOLECULAR CONDUCTORS

The material λ-(BETS)$_2$FeCl$_4$ is remarkable for the observation few years ago of the Jaccarino-Peter (JP) effect—the field-induced superconductivity. That occurs because the exchange coupling between the irons' spins and those of the conducting electrons of the (BEDT)-skeleton bears antiferromagnetic character. As the result, magnetization of Fe-ions leads to the *internal* magnetic field that acts on the conduction electrons' spins in the direction opposite to the applied external field. Y.J. Jo *et al*. studied the material at elevated pressure (to avoid JP effect) to investigate and measure the internal field through its direct manifestations, such as the spin-splitting of Fermi surfaces (FS). The Shubnikov-de Haas oscillations also revealed the appearance of the new, larger, FS orbit attributed to the magnetic breakdown between the closed-and open trajectories.

This research was published in **Physical Review B, 73**, 214532 (2006).

STUDY OF PRESSURE EFFECT ON THE INTERNAL FIELD OF THE FIELD-INDUCED ORGANIC SUPERCONDUCTOR λ-(BETS)$_2$FeCl$_4$

Y. J. Jo (Ewha W. Univ. & NHMFL), H. Y. Kang, W. Kang (Ewha W. Univ.); S. Uji, T. Terashima (NIMS); T. Tanaka, M. Tokumoto (AIST); A. Kobayashi (U. of Tokyo), H. Kobayashi (IMS)

INTRODUCTION

Study of BETS compounds containing Fe^{3+} magnetic ions has been of particular interest because the large magnetic moments of Fe^{3+} ions would induce the π-electron spins on donor molecules to develop a π-d coupled antiferromagnetic spin structure. Electrical resistivity and magnetic susceptibility measurements reveal that the π conduction electrons from BETS molecules and the localized magnetic moments of the anions coexist down to very low temperature. Measurement of the Shubnikov–de Haas (SdH) oscillations in λ-(BETS)$_2$FeCl$_4$ at ambient pressure revealed oscillations with two distinct

frequencies of 609 and 737 T. The splitting of the SdH oscillations is attributed to the spin-dependent FS separation due to the internal magnetic field, which is 32 T according to the spin-splitting factor of the Lifshitz-Kosevich formula. We have measured the SdH oscillations at a pressure of 6 kbar. Changes of the Fermi surface topology and the internal field with pressure are explored.

EXPERIMENTAL

Annealed gold wires were attached to the sample surfaces so that the current may flow along the least conducting b^* axis. Pressure was generated with a ultra-miniature BeCu pressure clamp cell. A 1:1 mixture of the Daphne 7373 oil and kerosene was used as a pressure medium. The pressure at low temperature was determined from the change of the superconducting T_c of high-purity lead (Pb). The experiments were performed in a 33 T resistive magnet at the NHMFL.

RESULTS AND DISCUSSION

Fig. 1(a) shows the oscillatory amplitude of the MR as a function of 1/H at several temperatures. The FFT spectra of the SdH oscillations between 18 and 33 T are displayed in Fig. 1(b). The splitting of both the α and β oscillations are observed. α_1, α_2, β_1, and β_2 have values of 803, 957, 3973, and 4255 T, respectively. The average effective masses are $(2.9\pm0.3)m_0$ for the α and $(5.5\pm0.3)m_0$ for the β orbit. For the closed-orbit oscillations, the effective mass falls from $4.1m_0$ to $2.9m_0$ with pressure. As for the MB orbit, the effective mass of $5.5m_0$ is lighter than that in other BETS compounds containing magnetic ions. Hydrostatic pressure will bring the BETS molecules closer together and hence broaden the energy band. So the decrease in effective mass with pressure is strongly related to the suppression of interaction between π electrons which depends critically on the bandwidth. As stated earlier, the internal field H_{int} can be directly calculated from the difference of frequencies, $2\Delta F$. Applying the expression for H_{int} to the α and β orbits, ΔF_α =77 T and ΔF_β=141 T, gives the estimated values for $H_{int,\alpha}$ =53 T and $H_{int,\beta}$=51 T, assuming the g factor of 2.

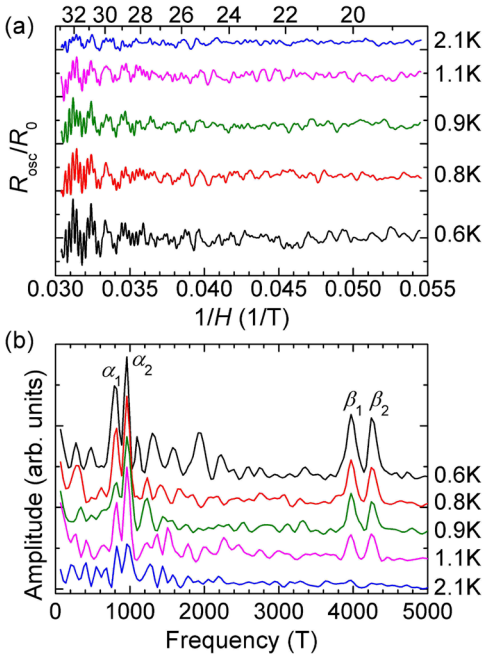

Figure 1.
(a) Oscillatory part of the magnetoresistance at 6 kbar. (b) FFT spectra of the SdH oscillations.

CONCLUSIONS

In λ-$(BETS)_2FeCl_4$ under pressure, new SdH oscillations with frequencies faster than those at ambient pressure, are detected and attributed to the magnetic breakdown orbit. The increase of the SdH frequencies indicates an increase in the size of the closed Fermi surface under pressure. The effective mass becomes smaller under pressure most likely due to the broadening of the bandwidth. The estimated internal field increases from 32 to 52 T under a pressure of 6 kbar.

REFERENCES

[1] Jo, Y. J., *et al.*, Phys. Rev. B, **73**, 214532 (2006).

QUANTUM FLUIDS

The manifold of Fractional Quantum Hall Effect (FQH) states is currently being investigated from the new viewpoint, namely, as an arena for realizations of some recent ideas related to the theory of quantum computing (QC).Two theoretical reports below address this issue.

Xin Wan *et al*. perform numerical studies for a model realization of the 5/2-FQH state. Fractionally charged quasiparticles for this filling factor are expected to obey the non-Abelian statistics (meaning, to put it simply, that at a permutation between the two quasiparticles in the plane the result depends on whether their rotation with respect to each other is performed in the clock or the counter-clock manner). Experimental methods, by which the non-ordinary properties of such a state should be seen, include tunneling experiments, which should involve chiral edge excitations. The authors find the provisions for observation of the non-trivial properties of the 5/2 filling FQH state in their realistic model for confinement.

This research was published in **Physical Review Letters, 97**, 256808 (2006).

The report of L. Hormozi *et al*. continues the previous work by the NHMFL and the Lucent Technologies group where they suggested a construction for two-qubit gates in the specific case of the so-called Fibonacci anions (see NHMFL Reports, 13 (4), 2006). In the current report the authors provide the mathematical results that also link the FQH effect with the theory of QC.

This research was published in **Physical Review Letters, 96**, 070503 (2006).

EDGE EXCITATIONS AND NON-ABELIAN STATISTICS IN THE MOORE-READ STATE: A NUMERICAL STUDY IN THE PRESENCE OF COULOMB INTERACTION AND EDGE CONFINEMENT

X. Wan (Zhejiang University, Hangzhou, China); K. Yang (NHMFL); E. H. Rezayi (Calstate LA)

INTRODUCTION

Fractional quantum Hall (FQH) liquids represent novel states of matter with non-trivial topological order. Consequences of such topological order include chiral edge excitations and fractionally charged bulk quasiparticles that obey Abelian or non-Abelian fractional statistics. It has been proposed that the non-Abelian quasiparticles can be used for quantum information storage and processing in an intrinsically fault-tolerant fashion, in which information is stored by the degenerate ground states in the presence of these non-Abelian quasiparticles, and unitary transformations in this Hilbert space can be performed by braiding the quasiparticles. While many Abelian FQH states have been observed and studied in detail, thus far there have been relatively few candidates for the non-Abelian ones. The most promising candidate is the FQH state at Landau level filling fraction 5/2, discovered two decades ago. The leading candidate for the ground state of this system is the Moore-Read (MR) paired state [1], which has been shown to support fractionally charged, non-Abelian quasiparticles [1]. The MR state received strong support from numerical studies using sphere and torus geometries. However these geometries do not contain any boundary, and are thus not suitable for study of edge states.

NUMERICAL CALCULATION AND RESULTS

In this work [2] we perform detailed numerical studies of edge excitations in the 5/2 FQH state in finite-size systems with disc geometry, taking into account the inter-electron Coulomb interaction and a semi-realistic model of the confining potential due to neutralizing background charge. We use a microscopic model of a two-dimensional electron gas (2DEG) confined to a two-dimensional disk, with neutralizing background charge distributed uniformly on a parallel disk of radius a at a distance *d* above the 2DEG. This distance parameterizes the strength of the confining potential, which decreases with increasing *d*. For filling fraction 5/2, we explicitly keep the electronic states in the first excited Landau level only, while neglecting the spin up and down electrons in the lowest Landau level, assuming they are inert. The amount of positive background charge is chosen to be equal to that of the half-filled first excited Landau level, so the system is neutral.

For a limited and very small range of *d*, we find the ground state does indeed have the same quantum number of, and has substantial overlap (up to 50%), with the MR state. Within this parameter space we are able to identify the existence of chiral fermionic and bosonic edge modes, in agreement with previous prediction. We find the fermionic mode velocity is much lower than that of the bosonic mode. With suitable short-range repulsive potential at the center, we show that a charge +e/4 quasihole can be localized at the center of the system, and its presence changes the spectrum of the fermionic edge mode. This confirms the existence and non-Abelian nature of such fractionally charged quasiparticles.

CONCLUSIONS

- In real system the MR state is likely to suffer from some forms of edge instability.
- A small change in confining potential (say by gating) may lead to qualitative change in edge properties.
- Fermionic mode velocity much lower than that of the bosonic mode; this may dramatically affect the propagation of e/4 quasiparticles at the edge.

ACKNOWLEDGEMENTS

This work is supported NSF grant No. DMR-0225698.

REFERENCES

[1] Moore, G. and Read, N. Nucl. Phys. B **360** (1991) 362.

[2] Wan, X., *et al.*, cond-mat/0609665 (Phys. Rev. Lett., in press).

QUANTUM COMPUTING WITH NONABELIAN QUASIPARTICLES

L. Hormozi, G. Zikos, N.E. Bonesteel (FSU Physics); S.H. Simon (Lucent Technologies)

INTRODUCTION

A remarkable recent development in the theory of quantum computation has been the realization that certain exotic states of matter in two space dimensions, so-called nonabelian states, may provide a natural medium for storing and manipulating quantum information. In these states, localized quasiparticle excitations have quantum numbers which are similar to ordinary spin quantum numbers. However, unlike ordinary spins, the quantum information associated with these quantum numbers is stored globally, throughout the entire system, and so is intrinsically protected against decoherence. Furthermore, these quasiparticles satisfy so-called nonabelian statistics. This means that when two quasiparticles are adiabatically moved around one another, while being kept sufficiently far apart, the action on the Hilbert space is represented by a unitary matrix which depends only on the topology of the path used to carry out the exchange. Topological quantum computation can then be carried out by

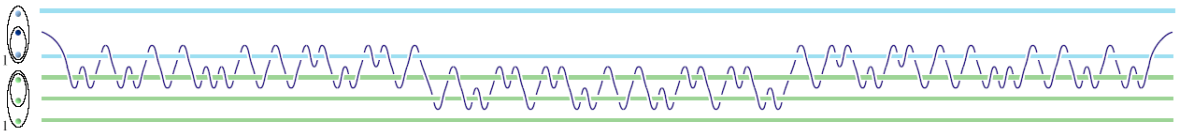

Figure 1.
A two-qubit gate construction for Fibonacci anyons in which a single quasiparticle moves.

moving quasiparticles around one another in two space dimensions. The quasiparticle world-lines form topologically nontrivial braids in three- (= 2 + 1) dimensional space-time, and because these braids are topologically robust (i.e., they cannot be unbraided without cutting one of the strands) the resulting computation is protected against error.

RESULTS AND DISCUSSION

In previous work[1], we showed how to construct two-qubit gates for a particular type of non-Abelian quasiparticles known as Fibonacci anyons (which may exist in the experimentally observed n=12/5 fractional quantum Hall effect) by "weaving" a pair of quasiparticles from one qubit (endoced into three quasiparticles) around the quasiparticles forming a second qubit. We have now given a mathematical proof that similar gate constructions are possible by moving only a *single* quasiparticle [2], and given explicit examples of such constructions [3] (e.g., see Fig. 1). We have also shown that there are fundamental limitations on generalizing these constructions to other kinds of non-Abelian quasiparticles, thus showing that Fibonacci anyons are particularly suited to topological quantum computation.

CONCLUSIONS

A central theme in all of our two-qubit gate constructions is that of breaking the problem of compiling braids for the six quasiparticles used to encode two qubits into a series of braids involving only three objects at a time. While these constructions do not produce the optimal braid of a given length which approximates a desired two-qubit gate, we believe they do lead to the most accurate two-qubit gates which can be obtained for a fixed amount of classical computing power.

Our explicit construction of braids which can used for universal quantum computation provides a direct, and constructive, proof of universality of Fibonacci anyons. This proof compliments the more abstract mathematical proofs of universality and confirms a surprising link between the theory of quantum computation and the physics of the fractional quantum Hall effect.

ACKNOWLEDGEMENTS

Work Supported by US DOE Grant # DE-FG02-97ER45639.

REFERENCES

[1] N.E. Bonesteel, *et al.*, Phys. Rev. Lett. **95** (2005) 140503.
[2] Simon, S.H., *et al.*, Phys. Rev. Lett. **96** (2006) 070503.
[3] Hormozi, L., *et al.*, Phys. Rev. B, in Press. (quant-ph/0610111).

CONDENSED MATTER

SEMICONDUCTOR PHYSICS

One vigorous activity at the NHMFL in this category is the use of magneto-photoluminescence (PL) to probe nanoscopic and quantum dot systems. Very evident is the increase in high quality, systematic investigations in pulsed field above 50T, where in particular, magneto-optics has played an important role. In this work of D. Andronikov *et al*., the observation of trions in quantum wells was performed in fields up to 87T.

In the research of B. M. Ashkinadze *et al.*, PL has been used to detect charge fractionalization in the magnetized two dimensional electron at fractional filling.

This research has been accepted for publication by the **International Journal of Modern Physics B.**

TRIONS IN CdTe/CdMgTe QUANTUM WELLS IN HIGH MAGNETIC FIELDS TO 87 T

D. Andronikov and V. Kochereshko (Ioffe Physical-Technical Institute, St-Petersburg, Russia);

G. Karczewski (Institute of Physics, Warsaw, Poland); S.A. Crooker (NHMFL, LANL)

INTRODUCTION

Magneto-optical spectroscopy is a powerful tool for studying negatively-charged excitons (trions) – charged three-particle complexes containing two electrons and one hole. Such complexes have two sets of states – singlet, with opposite electron spin alignment, and triplet, with parallel electron spins. It has been shown theoretically (e.g., [1]) and experimentally (e.g., [2]) that both singlet and triplet trion states increase their binding energies in magnetic field. Moreover the triplet state is unbound in the absence of a magnetic field. Thus application of an external magnetic field allows clear observation of the entire set of singlet and triplet trion states in optical spectroscopic experiments.

EXPERIMENTAL

In our earlier experiment [2] we have measured photoluminescence (PL) and reflectivity spectra of a 10 nm wide CdTe/$Cd_{0.7}Mg_{0.3}Te$ modulation-doped single quantum well containing 2D electron gas of a moderate density ($n_e \sim 3 \times 10^{10}$/ cm^2) in a magnetic field up to 45T at 1.6K, 4.2K, and 15K. Those measurements allowed us to classify the observed spectral signatures of singlet, as well as dark and bright triplet trion states. In our latest experiment we have performed PL measurements of a similar quantum well structure in magnetic field up to 87 T at liquid helium temperatures. Figure 1 (a) shows a set of PL spectra in magnetic field from 0 to 55 T in σ - circular polarization, Figure 2 demonstrates a PL spectra in the same polarization at the peak field of 87 T. These data were taken in the 60 T Long-Pulse magnet and the 100T Multi-Shot magnet, respectively.

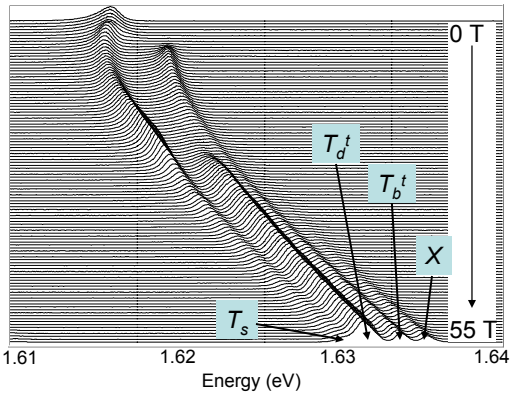

Figure 1.
(a) PL spectra of a CdTe/CdMgTe single quantum well structure taken in magnetic field from 0-55 T in σ - circular polarization. X indicates the neutral exciton line, T_s is a singlet trion line, T^t_d is the dark triplet trion line, and T^t_b is the bright triplet trion line.

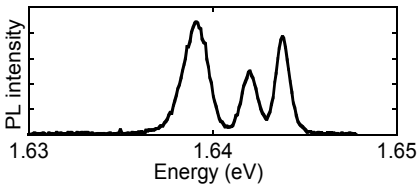

Figure 2.
A PL spectra of the same structure in σ^- circular polarization at 87 T magnetic field.

The acquired PL spectra have confirmed the conclusion about the kinetic nature of the trion states behavior made in our previous study: with increasing magnetic field the singlet trion state T_s is suppressed meanwhile the dark triplet state T^t_d is promoted and becomes one of the dominating lines in the PL spectra due to spin-dependent trion formation mechanism [2]. In our previous research we have been able to observe the bright triplet trion state T^t_b only as a shoulder to the neutral exciton line X. Here, at a very high magnetic field (>50 T) the bright triplet trion state T^t_b is observed as a separate spectral line. This is in agreement with theoretical calculations of the binding energy dependence of this state on magnetic field (e.g. [1]). Measurements of the trionic PL at a magnetic field as high as 87 T have been performed for the first time. Such experiment at an unprecedented magnitude of the magnetic field gives valuable information on the binding energy field dependences of all the observed states and could be used to verify binding energy calculations in the high field limit.

REFERENCES

[1] A.B. Dzyubenko, *et al*., Phys. Status Solidi B **227** (2001) 365.
[2] D. Andronikov, *et al.*, Phys. Rev. B **72**, (2005) 165339.

PHOTOLUMINESCENCE OF A HIGH MOBILITY 2DEG IN THE FRACTIONAL QUANTUM HALL EFFECT REGIME

B.M. Ashkinadze, E. Cohen (Technion, Haifa, Israel); D. Smirnov (NHMFL); L.N. Pfeiffer (Alcatel-Lucent Technologies, NJ)

INTRODUCTION

The electron-electron interaction strongly modifies the energy spectrum of the two-dimensional electron gas (2DEG) under a perpendicularly applied magnetic field (*B*), in the quantum Hall effect regime [1]. Various anomalies were observed in the PL spectrum at integer and fractional electron filling factors ν. However, PL line splitting due to the e-e interaction at ν<1, could hardly be resolved [2]. The reasons are either the photoexcited hole proximity to the 2DEG (in the case of modulation-doped quantum wells), or the broadening of the 2DEG-acceptor PL band in the case of Be-doped heterojunctions (HJs).

EXPERIMENTAL

We measured the magneto-PL spectra of several modulation doped, ultra-high mobility (μ_e> $5{\cdot}10^6$ $cm^2/V{\cdot}sec$ at 1 K) GaAs/AlGaAs single HJs at T=1.2-0.3 K. The 2DEG density varied in the range of $n_{2D}=(0.6\text{-}2.7){\cdot}10^{11}$ cm^{-2}. Low-density non-equilibrium electrons and holes were photo-exited at laser energies of 1.58 eV or 1.96 eV. An optical fiber and a polarizer inserted into the He3 cryostat were used for photoexcitation and collection of the circularly polarized PL. The magnetic field varied up to 25T.

RESULTS AND DISCUSSION

All studied HJs show PL peak energy and intensity anomalies at ν =2 and 1, similar to those previously reported for such HJs [3]. An abrupt transfer between free exciton and 2DEG-hole PL is observed at T<2K. It results from the change in the exciton dissociation rate and the appearance of free holes near the magnetized 2DEG for ν < 2.

The strong PL anomalies near ν=2/3 and 1/3 are clearly observed for the HJs with n_{2D}=1.6·10^{11} cm^{-2} (Fig. 1). These anomalies are seen only at the lowest temperature (0.3-0.4 K) and for HJs with n_{2D}>1·10^{11} cm^{-2}. Near ν=2/3, a PL line broadening occurs, and several PL lines can be revealed. The energy separation between the PL lines is ~ 0.1-0.15 meV. In the range of ν=2/5-1/3, the PL line splits into several lines with the energy separation of ~ 0.2-0.3 meV. It is important to notice that several HJs having various n_{2D} show similar PL structure at ν=2/5-1/3 and 2/3.

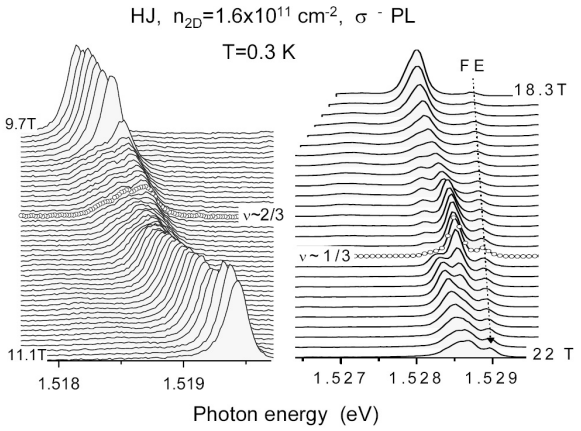

Figure 1.
Waterfall plot of the PL spectra of the HJ near ν=2/3 and 1/3 (n_{2D}= 1.6·10^{11} cm^{-2}.).

CONCLUSIONS

The obtained PL spectra clearly show splitting of the 2DEG-hole PL into several lines at fractional filling factor. We attribute this effect to a charge fractionalization of the magnetized 2DEG, when a hole can recombine with a quasiparticles and/or generate quasiholes in the incompressible 2DEG condensate.

ACKNOWLEDGEMENTS

B.M.A. acknowledges support from the NHMFL Visiting Scientist Program.

REFERENCES

[1] MacDonald, A.H. et.al, PRL 68 (1992) 1939; Parfit, M., et.al, PRB 68 (2003) 035306; Chen, X.M., et.al, PRB 50 (1994) 2354
[2] Goldberg, B.B., et.al, PRL 65 (1990) 641; Turberfield, A.J., et.al, PRL 65 (1990) 637
[3] Nicholas, R.J., et.al, Physica B249 (1998) 553; Ashkinadze, B.M., et.al, PRB 72 (2005) 075332

SPECIAL EDITION 2007 VOLUME 14 • NO. 2

SUPPORTED BY: THE NATIONAL SCIENCE FOUNDATION

1800 EAST PAUL DIRAC DRIVE
TALLAHASSEE, FL 32310-3706

TEL: 850 644-0311
FAX: 850 644-8350
www.magnet.fsu.edu

Non-Profit Organization U.S. Postage PAID Tallahassee, Fl Permit No. 55

Reviewing the 2006 NHMFL RESEARCH REPORTS

RESEARCH HIGHLIGHTS FROM:

Life Sciences
Chemistry
Magnet Science & Technology
Condensed Matter

NATIONAL HIGH MAGNETIC FIELD LABORATORY
FSU • UF • LANL